Publications of the Astronomical Society of the Pacific, **119**: 747–767, 2007 July

SIM PlanetQuest Key Project Precursor Observations to Detect Gas Giant Planets around Young Stars

Angelle Tanner,[1] Charles Beichman,[1] Rachel Akeson,[1] Andrea Ghez,[2] Konstantin N. Grankin,[3] William Herbst,[4] Lynne Hillenbrand,[5] Marcos Huerta,[6] Quinn Konopacky,[2] Stanimir Metchev,[2] Subhanjoy Mohanty,[7] L. Prato,[8] and Michal Simon[9]

Received 2007 April 23; accepted 2007 June 11; published 2007 July 12

ABSTRACT. We present a review of precursor observing programs for the *SIM PlanetQuest* Key Project devoted to detecting Jupiter-mass planets around young stars. In order to ensure that the stars in the sample are free of various sources of astrometric noise that might impede the detection of planets, we have initiated programs to collect photometry, high-contrast images, interferometric data, and radial velocities for stars in both the northern and southern hemispheres. We have completed a high-contrast imaging survey of target stars in Taurus and the Pleiades and found no definitive common proper motion companions within 1″ (140 AU) of the *SIM* targets. Our radial velocity surveys have shown that many of the target stars in Sco-Cen are fast rotators, and a few stars in Taurus and the Pleiades may have substellar companions. Interferometric data of a few stars in Taurus show no signs of stellar or substellar companions with separations of 5–50 mas. The photometric survey suggests that approximately half of the stars initially selected for this program are variable to a degree ($1\ \sigma > 0.1$ mag) that would degrade the astrometric accuracy achievable for that star. While the precursor programs are still a work in progress, we provide a comprehensive list of all targets and rank them according to their viability as a result of the observations taken to date. The observable that removes by far the most targets from the *SIM* young stellar object (YSO) program is photometric variability.

1. INTRODUCTION

The majority of the over 200 planets found to date have been detected using either radial velocity (RV) or transit studies in orbits ranging from less than 0.1 AU out to beyond 5 AU, with a wide range of eccentricities and with masses ranging from less than that of Uranus up to many times that of Jupiter (Butler et al. 2006). However, the host stars of these planets are mature main-sequence stars that were chosen based on their having quiescent photospheres for the successful measurement of small Doppler velocities (<10 m s^{-1}). Similarly, stellar photospheres must be quiescent at the millimagnitude level for transit detections, since a Jupiter-mass planet transiting a solar-type star reduces the photometric signal by about 1.4%. Since young stars often have radial velocity fluctuations or rotationally broadened line widths of *at least* 500 m s^{-1} and brightness fluctuations of many percents, RV measurements accurate to <100 m s^{-1} or transit observations cannot be used to detect planets around young stars.[10] A few potentially planetary-mass objects have been detected at 20–100 AU from young host stars (<10 Myr) by direct coronagraphic imaging; e.g., 2MASSW J1207334−393254 (Chauvin et al. 2005) and GQ Lup (Neuhäuser et al. 2005). However, these companions are only inferred to be of planetary mass by comparison to uncertain evolutionary models that predict the brightness of "young Jupiters" as a function of mass and age (Wuchterl & Tscharnuter 2003; Baraffe et al. 2003; Burrows et al. 1997). Since dynamical determinations of mass are impossible for objects on such distant orbits, it is difficult to be sure that these are planets and not brown dwarfs. Nor is it even clear that the origin of these distant "young Jupiters" is due to same formation processes that created planets found closer in. Multiple fragmentation events (Boss 2001), rather than core accretion in a dense disk (Ida & Lin 2004), may be responsible for the formation of these distant objects. As a result of the selection biases of the radial velocity, transit, and direct-imaging tech-

[1] Michelson Science Center, California Institute of Technology, Pasadena, CA; angelle.tanner@jpl.nasa.gov.
[2] Division of Astronomy, University of California at Los Angeles, Los Angeles, CA.
[3] Astronomical Institute of the Uzbek Academy of Sciences, Tashkent, Uzbekistan.
[4] Astronomy Department, Wesleyan University, Middletown, CT.
[5] California Institute of Technology, Pasadena, CA.
[6] Department of Astronomy, University of Florida, Gainesville, FL.
[7] Center for Astrophysics, Harvard University, Cambridge, MA.
[8] Lowell Observatory, Flagstaff, AZ.
[9] Department of Physics and Astronomy, State University of New York at Stony Brook, Stony Brook, NY.

[10] A number of groups are attempting RV observations in the near-IR, since at these wavelengths it may be possible to improve on these limits and find a few "hot Jupiters" within 0.1 AU.

niques, we know little about the incidence of close-in planets around young stars, leaving us with many questions about the formation and evolution of gas giant planets.

Given the observational limitations and uncertainties that are inherent to radial velocity and direct-imaging surveys, microarcsecond astrometry is a feasible and direct method for estimating the masses of giant planets around stars in young clusters that lie at distances closer than 140 pc (Beichman 2001). Equation (1) gives the astrometric amplitude ϕ in units appropriate to the search for planets around young stars:

$$\phi = 35 \frac{140\ \mathrm{pc}}{D_{\mathrm{pc}}} \frac{a_{\mathrm{AU}}}{5.2\ \mathrm{AU}} \frac{M_p}{M_J} \frac{M_\odot}{M_\star}\ \mu\mathrm{as}, \qquad (1)$$

where ϕ is the astrometric amplitude in μas, D is the distance to the star in parsecs, a is the orbital semimajor axis of the planet in AU, M_p is the planet mass in Jupiter masses, and $M_\star$ is the star's mass in solar masses. Thus, a Jupiter orbiting 5.2 AU away from a 0.8 $M_\odot$ star at a distance of the youngest stellar associations (1–10 Myr), such as Taurus and Chamaeleon 140 pc away, would produce an astrometric amplitude of 44 μas. At the 25–50 pc distance of the nearest young stars (10–50 Myr), such as members of the β Pic and TW Hya moving groups, the same system would have an astrometric amplitude in excess of 100 μas. Moving a Jupiter into a 1 AU orbit would reduce the signal by a factor of 5.2, or 50 μas, for a star at 25 pc, and 8 μas for one in Taurus. Table 1 lists the star formation regions and young moving groups being included in the *SIM*-YSO survey, a *SIM PlanetQuest* Key Project aimed at detecting Jupiter-mass planets around young stars. Since *SIM* will be able to detect astrometric signals with a single-measurement accuracy (SMA) of 4 μas (1 σ) in a fairly quick "narrow angle" (NA) observation, and 11 μas in a single "wide angle" (WA) observation, a search for gas giants falls well within *SIM*'s capabilities for wide- and narrow-angle astrometry and forms the core of the *SIM*-YSO program. With *SIM*'s sensitivity, it is reasonable to study stars brighter than $R \sim 12$ mag to a level such that the expected astrometric amplitude of 8 μas for stars at 140 pc is detected with 2 σ confidence in each measurement. This astrometric accuracy is appropriate for detecting planets of unknown orbital parameters with a series of approximately 75–100 one-dimensional measurements (Sozzetti et al. 2003; Catanzarite et al. 2006).

Figure 1 shows orbital location (semimajor axis) and $M \sin i$ for over 200 known planets orbiting nearby mature stars.[11] These planets were found using radial velocity measurements with noise levels as low as 1 m s^{-1}. However, for the young stars considered here, the radial velocity measurements will be limited, even in the near-infrared, to 100–500 m s^{-1} (or greater), due to rapid rotation, veiling, and photospheric variability. Thus, we plot a RV sensitivity curve for planets orbiting a 1 $M_\odot$ star, assuming a limiting accuracy of 100 m s^{-1}. For comparison, we plot the astrometric sensitivity curve for our *SIM*-YSO project, where we demand that the minimum detectable planet have an amplitude of at least 8 μas. The curve is plotted for a 1 $M_\odot$ star located at the distance of Taurus (140 pc). For planets with periods greater than the nominal mission duration of 5 years, we have degraded the sensitivity as shown schematically in the plot. Finally, we estimate how a coronagraph on a 30 m telescope or an interferometer with an 85 m baseline, both operating at 1.6 μm and reaching down to the Jovian-mass range at orbital distances of 10 AU or greater, would complement but not replace *SIM* observations.

[11] Planet information from the Extrasolar Planets Encyclopaedia at http://exoplanet.eu (J. Schneider, 2007).

TABLE 1
SIM-YSO SAMPLE

Cluster	Age (Myr)	Distance (pc)	No. of Stars
β Pic	20	10–50	16
Chameleon	1–10	140	8
η Cha	4–7	100	2
Horologium	30	60	12
IC 2391	53	155	12
Ophiuchus	2	160	5
Pleiades	125	130	14
TW Hydra	10	60	15
Taurus-Aureiga	2	140	25
Tucanae	20	45	20
Upper Sco	1–10	145	49
Sco Cen	1–25	130	81

In order to maximize the scientific yield of this *SIM* key project, a significant effort is required to gather information about the target stars prior to the launch of *SIM*. A careful vetting of the target list is required in order to reject stars that might be problematic due to either the presence of starspots that might induce large astrometric offsets, the presence of circumstellar emission from scattered light, or the presence of visible or spectroscopic companions.

To ensure that we observe astrometrically stable systems, we have initiated a series of precursor observations to check for nearby infrared companions (§ 3), radial velocity variations due to unseen companions (§ 4), and photometric variability (§ 5). Table 2 summarizes the precursor programs currently being conducted, including the telescopes and the principal investigators. In subsequent sections, we summarize the different programs and give detailed results from a number of them. The *SIM*-YSO target list will continue to evolve as we add new stars for their scientific interest and remove stars due to one failing or another. In the end, we intend to have a complete sample in both stellar age and mass that will allow for a statistically significant study of planets around young stars.

This paper describes the present status of the *SIM*-YSO sample, the overall strategy for the precursor vetting program, and detailed results of one specific program, the Palomar AO survey, aimed at identifying companions to the *SIM*-YSO targets in the Pleiades and Taurus. We summarize briefly the progress

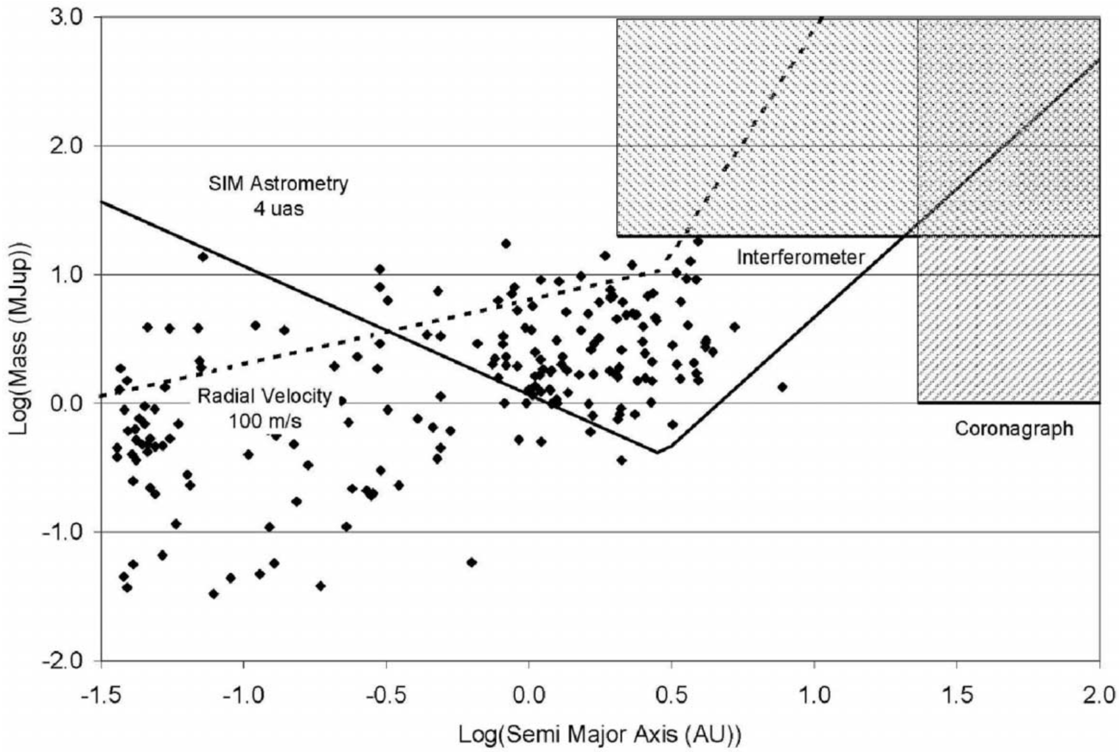

FIG. 1.—Plot of planet mass in M_J vs. semimajor axis of the sensitivities expected from the *SIM*-YSO survey (*solid line*), in addition to ground-based coronagraph (*labeled*), interferometry (*labeled*), and radial velocity (*dashed line*) surveys of young stars. Also plotted are the properties of the known radial velocity planets (*diamonds*). All these sensitivity limits assume a distance of 140 pc.

being made on our photometric and radial velocity surveys of both the northern and southern targets, and their implications for the *SIM*-YSO target sample.

2. THE *SIM*-YSO STELLAR SAMPLE OF YOUNG STARS

In a survey of ~200 young stars, we expect to find anywhere from 10–20 to 200 planetary systems, depending on whether the 5%–10% of stars with known radial velocity planets are representative of the younger planet population, or whether all young stars have planets, only to lose them to inward migration. The youngest stars in the sample (see Table 1) will be located in well-known star-forming regions and will be observed in narrow-angle mode, which is capable of achieving SMAs of 4 μas. Somewhat older stars, such as those in the β Pictoris and TW Hydrae associations, are only 25–50 pc away and can be observed less expensively in a wide-angle mode capable of SMAs of <11 μas (Unwin 2005).

We have set our sensitivity threshold to ensure the detection of Jupiter-mass planets in the critical orbital range of 1 to 5 AU. These observations, when combined with the results of the *SIM* planetary searches of mature stars, will allow us to test theories of planetary formation and early solar system evolution. By searching for planets around pre–main-sequence stars carefully selected to span an age range from 1 to 100 Myr, we will learn at what epoch and with what frequency

TABLE 2
PRECURSOR PROGRAMS

Program	Telescope	PI
AO imaging (north) …………………	Palomar	A. Tanner
AO imaging (south) …………………	VLT	C. Dumas
Speckle imaging (north) ……………	Keck	A. Ghez, Q. Konopacky
Interferometric visibilities (north) ……	Keck	R. Akeson
RV survey (north) …………………	McDonald	L. Prato
RV survey (south) …………………	CTIO/Magellan	S. Mohanty
Photometry (north) …………………	Maidanak	K. Grankin
Photometry (south) …………………	SMARTS	M. Simon

giant planets are found at the water-ice "snow line," where they are expected to form (Pollack et al. 1996). This will provide insight into the physical mechanisms by which planets form and migrate from their place of birth, as well as their survival rate. With these observations in hand, we will provide data, for the first time, on such important questions as: What processes affect the formation and dynamical evolution of planets? When and where do planets form? What is the initial mass distribution of planetary systems around young stars? How might planets be destroyed? What is the origin of the eccentricity of planetary orbits? What is the origin of the apparent dearth of companion objects between planets and brown dwarfs seen in mature stars? How might the formation and migration of gas giant planets affect the formation of terrestrial planets?

Our observational strategy is a compromise between the desire to extend the planetary-mass function as low as possible and the essential need to build up sufficient statistics on planetary occurrence. About half of the sample will be used to address the "where" and "when" of planet formation. We will study classical T Tauri stars (CTTSs) that have massive accretion disks, as well as postaccretion, weak-lined T Tauri stars (WTTSs). Preliminary estimates suggest the sample will consist of ~30% CTTSs and ~70% WTTSs, driven in part by the difficulty of making accurate astrometric measurements toward objects with strong variability or prominent disks. The extent to which this distribution of CTTSs and WTTSs survives the screening programs for photometric and dynamic stability is addressed in § 6. The second half of the sample will be drawn from the closest young clusters with ages starting around 5 Myr to the 10 Myr point thought to mark the end of prominent disks, and ending around the 100 Myr age, at which theory suggests that the properties of young planetary systems should become indistinguishable from those of mature stars. The properties of the planetary systems found around stars in these later age bins will be used to address the effects of dynamical evolution and planet destruction (Lin 2001).

We have adopted the following criteria in developing our initial list of candidates: (1) stellar mass between 0.2 and 2.0 $M_{\odot}$, (2) $R < 12$ mag for reasonable integration times, (3) distance less than 140 pc to ensure an astrometric signal greater than 6 μas, (4) no companions within 2″ and 100 AU for instrumental and scientific considerations, respectively, (5) no nebulosity to confuse the astrometric measurements, (6) variability $\Delta R < 0.1$ mag, and (7) a spread of ages between 1 and 100 Myr to encompass the expected time period of planet-disk and early planet-planet interactions. With proper selection, the effect of various astrophysical disturbances can be kept to less than the few μas needed to detect Jupiter-mass planets at ~50–140 pc.

The initial *SIM*-YSO sample (see Table 3) consists of stars in the well-known star-forming regions and close associations. Figure 2 shows histograms of the properties of the stars in the sample, including distance, *V* magnitude, and age. The stars included in the initial sample have been screened for binarity in either imaging (Stauffer et al. 1998; Lowrance et al. 2005) or spectroscopic surveys (White & Ghez 2001; Mathieu et al. 1997; Steffen et al. 2001).

3. HIGH-CONTRAST DIRECT IMAGING

We begin by presenting the results of a companion survey for the *SIM*-YSO targets in our Taurus and Pleiades samples (see Table 4). Companions within the 1.5″ field of view of the *SIM* interferometer that have magnitudes within $\Delta V \sim 4$ mag (M. Shao 2007, private communication) could cause a bias in the position of the fringe used to make the astrometric measurements. In addition, a massive unknown stellar companion will induce astrometric perturbations, complicating the astrometric solution for a planet around the primary star. To look for common proper motion companions to the *SIM*-YSO stars, we have conducted an adaptive optics (AO) coronagraphic imaging survey around 31 stars in the Taurus (2 Myr, 140 pc; Kenyon et al. 1994) and Pleiades (120 Myr, 135 pc; Stauffer et al. 1998; Pan et al. 2004) clusters with the Palomar Adaptive Optics (PALAO) system and its near-infrared Palomar High Angular Resolution Observer (PHARO) camera on the Hale 200 inch (5 m) telescope (Hayward et al. 2001). These data will reveal the presence of stellar and brown dwarf companions located between ~50 and 1000 AU, and in the case of the youngest stars in these systems (~2 Myr), will be sensitive to hot, young planets with masses in the range of $10M_J$–$20M_J$ (Burrows et al. 1997; Baraffe et al. 2003).

In the process of searching for unseen companions around these stars, we are also addressing planet formation issues. By investigating whether the "brown dwarf desert" observed for separations of <5 AU around main-sequence stars (Marcy & Butler 2000) also exists at larger separations for young stars, we can test whether brown dwarfs are formed at this separation and subsequently migrate inward and are destroyed by falling onto the star. In this case, we might find that T Tauri stars have a larger population of brown dwarfs than main-sequence stars at these separations.

3.1. Data Reduction and Analysis

The Palomar observations were obtained over three observing runs (2003 October 23, 2003 December 4–6, and 2005 November 12–14), with good (0.2″) to moderate (0.5″) seeing throughout the nights. The PHARO-PALAO camera has a pixel scale of 25 mas pixel^{-1} and a field of view of 25″. Each target was observed with the 0.97″ diameter occulting spot placed over the star, with integration times of 60 s each and multiple (10–20) images collected per target. Sky images were also taken adjacent to each set of target images by offsetting 30″ from the target in the four cardinal directions. For flux calibration, observations of the target stars were taken with the star offset from the coronagraph in a five-point dither pattern to allow for adequate sky subtraction. To improve observing efficiency, those stars with similar magnitudes and colors were

TABLE 3
SIM-YSO SAMPLE

Name	Cluster	Distance (pc)	Spectral Type	Age (Myr)	Star Mass[a] ($M_\odot$)	Signal (μas)	T Tauri Class	V (mag)	2MASS K_s (mag)
Low-Variability Targets									
PreibZinn 9964[b]	U Sco	145	M1	0.1	0.3	23.68	…	…	8.36
51 Eri	β Pic	29.8	F0 V	20	1.5	21.51	…	5.22	4.54
PreibZinn 9914	U Sco	145	M0.5	0.5	0.3	19.50	…	…	9.09
RECX 10	η Cha	100	K6	7	0.6	17.48	WTT	12.53	8.73
PreibZinn 9928	U Sco	145	M0	1	0.4	15.79	…	…	8.80
PreibZinn 9913	U Sco	145	M0	1.2	0.4	15.07	…	…	8.88
PreibZinn 9919	U Sco	145	K6	0.7	0.5	12.51	…	…	8.11
PreibZinn 9974	U Sco	145	K4	0.5	0.6	10.36	…	…	8.46
PreibZinn 9936	U Sco	145	K7	2.7	0.7	10.20	…	…	9.12
PreibZinn 9967	U Sco	145	K5	1.1	0.7	10.05	…	…	8.56
PreibZinn 9969	U Sco	145	K5	1.8	0.7	9.47	…	…	8.56
HII 489	Pleiades	130	F8	125	…	9.25	…	10.38	8.87
HII 1794	Pleiades	130	F8	125	…	9.25	…	10.20	8.89
HII 2366	Pleiades	130	G2	125	…	9.25	…	11.53	9.55
TYC 8283-2795-1	Sco-Cen (UCL)	130		…	…	9.25	WTT	10.79	8.98
PreibZinn 9950	U Sco	145	K5	2.5	0.8	8.84	…	…	8.90
L1551-55	Tau Aur	140	K7	2	…	8.59	…	13.22	9.31
PreibZinn 9939	U Sco	145	K4	2.2	0.8	8.29	…	…	8.73
HII 1124	Pleiades	130	K3 V	125	1.0	7.79	…	12.12	9.86
PreibZinn 9958	U Sco	145	K2	1.2	0.9	7.62	…	…	8.43
HII 1095	Pleiades	130	K0 V	125	1.0	7.40	…	11.92	9.67
HII 1309	Pleiades	130	F6 V	125	1.0	7.40	…	9.58	8.28
HII 1613	Pleiades	130	F8 V	125	1.0	7.40	…	9.87	8.57
HII 1797	Pleiades	130	F9 V	125	1.0	7.40	…	10.09	15.04
HII 1856	Pleiades	130	F8 V	125	1.0	7.40	…	10.20	8.66
TYC 8654-1115-1	Sco-Cen (LCC)	130		24	1.0	7.40	WTT	10.21	8.13
TYC 8295-1530-1	Sco-Cen (UCL)	130	G5	21	1.0	7.40	WTT	10.98	8.90
PreibZinn 9945	U Sco	145	K2	1.2	0.9	7.37	…	11.17	8.04
HD 141569	None	35	B9.5e	5	4.0	6.87	…	7.11	6.82
TYC 8667-283-1	Sco-Cen (LCC)	130	G3/G5 V	23	1.1	6.72	WTT	9.31	7.62
TYC 7783-1908-1	Sco-Cen (LCC)	130	G8 IV:	18	1.1	6.72	WTT	9.82	7.51
TYC 8258-1878-1	Sco-Cen (LCC)	130		15	1.1	6.72	WTT	10.62	8.27
TYC 9244-814-1	Sco-Cen (LCC)	130	G3/G5 III	22	1.1	6.72	WTT	10.21	8.40
TYC 8270-2015-1	Sco-Cen (UCL)	130		17	1.1	6.72	WTT	10.91	8.69
TYC 7851-1-1	Sco-Cen (UCL)	130	G9	17	1.1	6.72	WTT	10.63	8.36
TYC 7353-2640-1	Sco-Cen (UCL)	130		18	1.1	6.72	WTT	10.72	8.67
CHXR 8	Cham	140	G0	100	1.1	6.24	WTT	11.45	9.73
HII 430	Pleiades	130	G8 V	125	1.2	6.16	…	11.40	9.47
HII 1032	Pleiades	130	A2	125	1.2	6.16	…	11.10	9.16
HII 1136	Pleiades	130	G7 V	125	1.2	6.16	…	12.02	12.14
HII 1275	Pleiades	130	K0 V	125	1.2	6.16	…	11.47	9.53
TYC 8646-166-1	Sco-Cen (LCC)	130		11	1.2	6.16	WTT	10.50	8.18
TYC 8636-2515-1	Sco-Cen (LCC)	130		11	1.2	6.16	WTT	10.58	8.12
TYC 8633-508-1	Sco-Cen (LCC)	130	K2 IV:+	16	1.2	6.16	WTT	9.41	7.65
TYC 9245-617-1	Sco-Cen (LCC)	130		10	1.2	6.16	WTT	10.01	7.55
TYC 8652-1791-1	Sco-Cen (LCC)	130	F6/F7	16	1.2	6.16	WTT	10.35	8.48
TYC 8259-689-1	Sco-Cen (LCC)	130		14	1.2	6.16	WTT	10.48	8.10
TYC 8248-539-1	Sco-Cen (LCC)	130	G1/G2	26	1.2	6.16	WTT	10.10	8.54
HD 120411	Sco-Cen (UCL)	130	G1 V	20	1.2	6.16	WTT?	9.79	8.16
V1009 Cen	Sco-Cen (UCL)	130	G8/K0 V	13	1.2	6.16	WTT?	10.18	7.95
TYC 7310-2431-1	Sco-Cen (UCL)	130	G5	16	1.2	6.16	WTT	10.36	8.28
TYC 8297-1613-1	Sco-Cen (UCL)	130		17	1.2	6.16	WTT	10.22	8.51
TYC 7822-158-1	Sco-Cen (UCL)	130	K1	13	1.2	6.16	WTT	11.11	8.51
TYC 7848-1659-1	Sco-Cen (UCL)	130	G5	15	1.2	6.16	WTT	10.36	8.21
HD 140421	Sco-Cen (UCL)	130	G1 V	17	1.2	6.16	WTT?	9.46	7.87
TYC 8317-551-1	Sco-Cen (UCL)	130	G0	13	1.2	6.16	WTT	10.29	8.27
TYC 7333-1260-1	Sco-Cen (UCL)	130	G1/G2 V	18	1.2	6.16	WTT	9.58	8.07
PreibZinn 9922	U Sco	145	G0	18	1.1	6.03	…	…	8.77
TYC 9231-1566-1	Sco-Cen (LCC)	130	G3 IV	12	1.3	5.69	WTT	9.23	7.18
TYC 8263-2453-1	Sco-Cen (UCL)	130	F8/G0 V	14	1.3	5.69	WTT	9.69	7.94

TABLE 3 (*Continued*)

Name	Cluster	Distance (pc)	Spectral Type	Age (Myr)	Star Mass[a] $(M_\odot)$	Signal (μas)	T Tauri Class	V (mag)	2MASS K_s (mag)
TYC 7813-224-1	Sco-Cen (UCL)	130		14	1.3	5.69	WTT	10.55	8.39
TYC 8683-242-1	Sco-Cen (UCL)	130		8	1.3	5.69	WTT	10.80	8.30
TYC 7828-2913-1	Sco-Cen (UCL)	130		5	1.3	5.69	WTT	11.02	8.29
TYC 7310-503-1	Sco-Cen (UCL)	130	K3	2	1.3	5.69	WTT	10.88	7.87
TYC 7845-1174-1	Sco-Cen (UCL)	130	K1	3	1.3	5.69	WTT	10.61	7.93
TYC 7349-2191-1	Sco-Cen (UCL)	130		1	1.3	5.69	WTT	11.09	8.29
PreibZinn 9975	U Sco	145	G9	1	1.2	5.62	…	10.50	7.43
HII 1514	Pleiades	130	G5 V	125	1.4	5.28	…	10.48	8.95
HD 140374	Sco-Cen (UCL)	130	G8 V	8	1.4	5.28	WTT?	9.69	7.80
CHXR 6	Cham	140	K2	1	1.3	5.28	CTT	11.22	7.31
PreibZinn 9979	U Sco	145	G5	9	1.3	5.18	…	…	8.69
High-Variability Targets									
PreibZinn 9980	U Sco	145	M1	0.3	0.3	22.87	…	…	7.91
PreibZinn 9940	U Sco	145	M2	0.4	0.3	22.10	…	…	8.61
PreibZinn 9970	U Sco	145	M1	0.5	0.3	20.72	…	…	8.82
PreibZinn 9955	U Sco	145		0.5	0.3	20.09	…	…	8.10
PreibZinn 9933	U Sco	145	M1	0.8	0.4	18.95	…	…	8.84
RECX 4	η Cha	100	K7	4	0.5	18.49	WTT	12.79	8.62
PreibZinn 9921	U Sco	145	M1	0.8	0.4	18.42	…	…	8.63
PreibZinn 993	U Sco	145	M1	1	0.4	17.45	…	…	9.08
PreibZinn 996	U Sco	145	M0	1	0.4	15.42	…	…	8.98
PreibZinn 9963	U Sco	145	M0	1.8	0.5	14.74	…	…	8.44
DM Tau	τ Aur	140	K5 V:e	2	0.5	14.61	CTT	13.78	9.52
PreibZinn 9959	U Sco	145	M0	2	0.5	14.11	…	…	8.91
PreibZinn 9962	U Sco	145	M0	2	0.5	14.11	…	…	8.92
CHXR 29	Cham	140	A0pshe	…	0.5	13.74	CTT	8.44	5.94
CHXR 18N	Cham	140	K1	…	0.5	13.74	WTT	12.05	7.77
CHXR 68A	Cham	140		…	0.5	13.74	WTT	13.37	8.87
T Cha	Cham	140	F5	…	0.5	13.74	CTT	11.86	6.95
PreibZinn 9911	U Sco	145	K7	0.8	0.5	13.26	…	…	8.37
PreibZinn 9916	U Sco	145	M0	2.9	0.5	13.26	…	…	9.27
DN Tau	τ Aur	140	K6 V:e	0.46	0.6	12.26	CTT	12.53	8.02
IP Tau	τ Aur	140	M0: Ve	2	0.6	11.84	CTT	13.04	8.35
PreibZinn 9926	U Sco	145	K7	1.8	0.6	11.05	…	…	8.92
DG Tau	τ Aur	140	G V:e	2	0.7	10.57	CTT	…	6.99
PreibZinn 9961	U Sco	145	K5	1.8	0.7	9.47	…	…	8.62
UY Aur	τ Aur	140	G5 V:e	2	0.7	9.28	CTT	12.40	7.24
BP Tau	τ Aur	140	K5 V:e	0.6	0.8	9.16	CTT	11.96	7.74
GK Tau	τ Aur	140		2	0.8	9.16	CTT	12.50	7.47
AA Tau	τ Aur	140	M0 V:e	2	0.8	9.04	CTT	12.82	8.05
HQ Tau	τ Aur	140		0.69	0.8	9.04	CTT	…	7.14
IW Tau	τ Aur	140	K7 V	2	0.8	9.04	WTT	12.51	8.28
DR Tau	τ Aur	140	K4 V:e	2	0.8	9.04	CTT	13.60	6.87
V830 Tau	τ Aur	140	K7	2	0.8	8.92	WTT	12.21	8.42
DL Tau	τ Aur	140	G V:e	2	0.8	8.92	CTT	13.55	7.96
L1551-51	τ Aur	140	K7	2	…	8.59	…	12.06	8.85
CI Tau	τ Aur	140	G V:e	2	…	8.59	…	12.99	7.79
V836 Tau	τ Aur	140	K7 V	2.1	0.8	8.59	WTT	13.13	8.60
PreibZinn 9918	U Sco	145	K3	1	0.8	8.50	…	…	8.33
PreibZinn 9942	U Sco	145	K5	2.9	0.8	8.50	…	…	8.37
PreibZinn 9984	U Sco	145	K3	1	0.8	8.50	…	…	8.93
TYC 8648-446-1	Sco-Cen (LCC)	130		19	0.9	8.22	WTT	11.18	8.79
PreibZinn 9968	U Sco	145	K2	1	0.8	7.89	…	11.65	7.69
SR 4/V2058 Oph	Ophiuchus	160	K5e	2	…	7.51	…	13.60	7.52
DoAr21 Oph	Ophiuchus	160	B2 V	2	…	7.51	…	13.82	6.23
Haro 1-16 Oph	Ophiuchus	160	K3	2	…	7.51	…	12.59	7.61
V1121 Oph	Ophiuchus	160	K5	2	…	7.51	…	11.25	6.96
V966 Cen	Sco-Cen (LCC)	130	K1: V:+	…	1.0	7.40	WTT?	9.76	8.08
TYC 7319-749-1	Sco-Cen (UCL)	130	K0	20	1.0	7.40	WTT	10.59	8.34
GI Tau	τ Aur	140	K5e	2	0.9	7.39	CTT	13.50	7.89
PreibZinn 991	U Sco	145	K3	3	0.9	7.37	…	…	9.43
PreibZinn 9937	U Sco	145	K4	4	0.9	7.37	…	…	8.93

TABLE 3 (*Continued*)

Name	Cluster	Distance (pc)	Spectral Type	Age (Myr)	Star Mass[a] ($M_\odot$)	Signal (μas)	T Tauri Class	V (mag)	2MASS K_s (mag)
PreibZinn 9976	U Sco	145	K1	1.2	1.0	6.98	…	…	8.49
V1072 Tau/TAP 35	τ Aur	140	K1	2	1.0	6.87	…	10.30	8.30
TYC 8640-2515-1	Sco-Cen (LCC)	130		20	1.1	6.72	WTT	10.77	8.73
TYC 8242-1324-1	Sco-Cen (LCC)	130	G0	16	1.1	6.72	WTT	10.38	8.14
TYC 8238-1462-1	Sco-Cen (LCC)	130	K0	21	1.1	6.72	WTT	10.10	8.01
TYC 8655-149-1	Sco-Cen (LCC)	130		19	1.1	6.72	WTT	10.31	8.37
TYC 8282-516-1	Sco-Cen (UCL)	130		19	1.1	6.72	WTT	10.68	8.54
TYC 7833-2559-1	Sco-Cen (UCL)	130	G6/G8 III/IV	21	1.1	6.72	WTT	10.61	8.45
TYC 8694-1685-1	Sco-Cen (UCL)	130		18	1.1	6.72	WTT	10.21	8.01
PreibZinn 9944	U Sco	145	K2	3.7	1.0	6.63	…	…	8.51
PreibZinn 9973	U Sco	145	K0	0.8	1.0	6.57	…	11.00	7.49
PreibZinn 9978	U Sco	145	K0	0.3	1.0	6.50	…	10.80	7.46
PreibZinn 9929	U Sco	145	K3e	3	1.1	6.32	…	13.40	8.52
PreibZinn 9954	U Sco	145	M3	3	1.1	6.32	…	…	8.86
TYC 9246…71-1	Sco-Cen (LCC)	130	G	7	1.2	6.16	CTT	10.54	7.29
TYC 9212-2011-1	Sco-Cen (LCC)	130		6	1.2	6.16	WTT	10.49	7.79
TYC 8644-340-1	Sco-Cen (LCC)	130		13	1.2	6.16	WTT	10.29	7.97
TYC 8645-1339-1	Sco-Cen (LCC)	130		5	1.2	6.16	WTT	10.82	7.73
TYC 8249-52-1	Sco-Cen (LCC)	130	K0/K1	13	1.2	6.16	WTT	10.48	8.13
HD 117524	Sco-Cen (LCC)	130	G5/G6 V	15	1.2	6.16	WTT?	9.84	7.83
TYC 7796-1788-1	Sco-Cen (UCL)	130	K5	13	1.2	6.16	WTT	10.17	7.88
TYC 7811-2909-1	Sco-Cen (UCL)	130		14	1.2	6.16	WTT	10.80	8.40
TYC 8283-264-1	Sco-Cen (UCL)	130		18	1.2	6.16	WTT	10.09	7.90
TYC 7824-1291-1	Sco-Cen (UCL)	130	G8 IV:	15	1.2	6.16	WTT	9.80	7.81
TYC 8294-2230-1	Sco-Cen (UCL)	130	G7	17	1.2	6.16	WTT	10.79	8.71
TYC 7852-51-1	Sco-Cen (UCL)	130	F7 V	18	1.2	6.16	WTT	9.05	7.69
PreibZinn 9986	U Sco	145	K0	1.8	1.1	6.14	…	…	7.76
PreibZinn 9983	U Sco	145	K0	2	1.1	6.03	…	…	8.51
PreibZinn 9971	U Sco	145	K1	2.5	1.1	5.92	…	11.65	8.09
TYC 8982-3213-1	Sco-Cen (LCC)	130	G1/G2 V	13	1.3	5.69	WTT	9.49	7.60
HD 105070	Sco-Cen (LCC)	130	G1 V	13	1.3	5.69	WTT?	8.89	7.31
TYC 8234-2856-1	Sco-Cen (LCC)	130		9	1.3	5.69	WTT	10.59	8.16
TYC 8633-28-1	Sco-Cen (LCC)	130	G2	15	1.3	5.69	WTT	9.49	7.77
HD 108568	Sco-Cen (LCC)	130	G1	14	1.3	5.69	WTT?	8.89	7.29
HD 113466	Sco-Cen (LCC)	130	G5 V:	14	1.3	5.69	WTT?	9.18	7.36
TYC 7815-2029-1	Sco-Cen (UCL)	130	K0/K1+	14	1.3	5.69	WTT?	9.46	7.88
TYC 7833-2037-1	Sco-Cen (UCL)	130	K1	10	1.3	5.69	WTT	11.23	8.73
TYC 7840-1280-1	Sco-Cen (UCL)	130	G9	9	1.3	5.69	WTT	10.57	8.29
PreibZinn 9949	U Sco	145	G7	8.5	1.2	5.53	…	…	8.46
LkCa 19	τ Aur	140	K0 V	2	1.3	5.49	WTT	10.85	8.15
PreibZinn 9925	U Sco	145	G9	4	1.2	5.44	…	10.99	8.44
TYC 8644-802-1	Sco-Cen (LCC)	130		6	1.4	5.28	WTT	10.21	7.66
HD 108611	Sco-Cen (LCC)	130	G5 V	10	1.4	5.28	WTT?	9.04	7.12
TYC 7326…28-1	Sco-Cen (UCL)	130	K1	7	1.4	5.28	WTT	10.54	8.12
HD 138995	Sco-Cen (UCL)	130	G5 V	10	1.4	5.28	WTT?	9.39	7.52
TYC 7842-250-1	Sco-Cen (UCL)	130		8	1.4	5.28	WTT	10.90	8.69
TYC 7333-719-1	Sco-Cen (UCL)	130	G8	10	1.4	5.28	WTT	10.99	8.53
TYC 7853-227-1	Sco-Cen (UCL)	130		8	1.4	5.28	WTT	11.05	8.65
Targets Yet to Be Measured									
GJ 803	β Pic	9.9	M1 Ve	20	0.4	242.81	…	8.81	4.53
HD 155555C	β Pic	31.4	M4.5	20	0.2	153.11	…	12.71	7.63
HIP 23309	β Pic	26.3	K7 V	20	0.5	81.25	…	10.02	6.24
HIP 3556	Tuc	45	M1.5	20	0.3	71.23	…	11.91	7.62
GJ 3305	β Pic	29.8	M0.5	20	0.5	64.53	…	10.59	6.41
CD −64 1208	β Pic	29.2	M0	20	0.6	54.88	…	9.54	6.10
GSC 8056-0482	Hor	60	M3 Ve	30	0.3	53.42	…	12.11	7.50
TWA 8A	TW Hya	60	M2	10	0.3	53.42	…	…	7.43
TWA 10	TW Hya	60	M2.5	10	0.3	53.42	…	…	8.19
TWA 11B	TW Hya	60	M2.5	10	0.3	53.42	…	13.30	5.77
HIP 107345	Tuc	45	M1	20	0.4	53.42	…	11.72	7.87
AO Men	β Pic	38.5	K3: V:	20	0.6	41.63	…	9.95	6.81
TWA 7	TW Hya	60	M1	10	0.4	40.06	…	11.06	6.90

TABLE 3 (*Continued*)

Name	Cluster	Distance (pc)	Spectral Type	Age (Myr)	Star Mass[a] ($M_\odot$)	Signal (μas)	T Tauri Class	V (mag)	2MASS K_s (mag)
TWA 13	TW Hya	60	M1 Ve	10	0.4	40.06	…	11.50	7.49
HD 35850	β Pic	26.8	F7 V	20	1.0	35.88	…	6.30	4.93
HIP 1993	Tuc	45	K7 V	20	0.6	35.61	…	11.26	7.75
GSC 8499-0304	Hor	60	M0 Ve	30	0.5	32.05	…	12.09	8.72
TWA 14	TW Hya	60	M0	10	0.5	32.05	…	…	8.50
TWA 18	TW Hya	60	M0.5	10	0.5	32.05	…	…	8.85
HD 3221	Tuc	45	K5 V	20	0.8	26.71	…	9.56	6.53
GSC 8497-0995	Hor	60	K6 Ve	30	0.6	26.71	…	10.97	7.78
TWA 6	TW Hya	60	K7	10	0.6	26.71	…	12.00	8.04
TWA 1	TW Hya	60	K8 Ve	10	0.6	26.71	…	10.92	7.30
TWA 19B	TW Hya	60	K7	10	0.6	26.71	…	…	8.28
V343 Nor	β Pic	39.8	K0 V	20	1.0	24.16	…	8.14	5.85
HD 202746	Tuc	45	K2 Vp	20	0.9	23.74	…	8.97	6.40
TWA 4	TW Hya	60	K5	10	0.7	22.89	…	8.89	5.59
TWA 9A	TW Hya	60	K5	10	0.7	22.89	…	11.13	7.85
TWA 17	TW Hya	60	K5	10	0.7	22.89	…	…	9.01
HD 1466	Tuc	45	F8/G0 V	20	1.0	21.37	…	7.46	6.15
HD 186602	Tuc	45	F7/F8 V	20	1.0	21.37	…	7.28	6.09
HD 207575	Tuc	45	F6 V	20	1.0	21.37	…	7.22	6.03
PPM 366328	Tuc	45	K0	20	1.0	21.37	…	9.67	7.61
GSC 8047-0232	Hor	60	K3 V	30	0.8	20.03	…	10.87	8.41
CD −53 386	Hor	60	K3 Ve	30	0.8	20.03	…	11.02	8.59
GSC 8862-0019	Hor	60	K4 Ve	30	0.8	20.03	…	11.67	8.91
β Pic	β Pic	19.3	A5 V	20	2.5	19.93	…	3.85	3.53
PZ Tel	β Pic	49.7	K0 Vp	20	1.0	19.35	…	8.43	6.37
HD 208233	Tuc	45	G8 V	20	1.2	17.81	…	8.90	6.75
CC Phe	Hor	60	K1 V	30	0.9	17.81	…	9.35	6.83
CD −65 149	Hor	60	K2 Ve	30	0.9	17.81	…	10.19	8.01
HD 172555	β Pic	29.2	A5 IV–V	20	2.0	16.46	…	4.78	4.30
HD 987	Tuc	45	G6 V	20	1.3	16.44	…	8.76	6.96
HR 9	β Pic	39.1	F2 IV	20	1.5	16.39	…	6.19	5.24
CPD −64 120	Hor	60	K1 Ve	30	1.0	16.03	…	10.29	8.01
HD 202917	Tuc	45	G5 V	20	1.4	15.26	…	8.65	6.91
HD 195627	Tuc	45	F1 III	20	1.5	14.25	…	4.75	4.04
HD 195961	Tuc	45	Fm	20	1.5	14.25	…	4.86	3.90
HD 164249	β Pic	46.9	F5 V	20	1.5	13.67	…	7.01	5.91
HD 207129	Tuc	45	G0 V	20	1.6	13.35	…	5.57	4.24
IQ Tau	τ Aur	140	M2	2	0.5	13.21	CTT	14.50	7.78
HD 181327	β Pic	50.6	F5/F6 V	20	1.5	12.67	…	7.04	5.91
HD 178085	Tuc	45	G0 V	20	1.7	12.57	…	8.31	6.88
RX J012320.9-572853	HOR	60	G6 V	30	1.3	12.33	…	8.53	6.85
DQ Tau	τ Aur	140	M0 V:e	2	0.6	12.05	CTT	13.66	7.98
RX J020718.6-531155	HOR	60	G5 V	30	1.4	11.45	…	8.64	6.89
TWA 19A	TW Hya	60	G3/G5 Vp	10	1.4	11.45	…	9.07	7.51
RX J020436.7-545320	HOR	60	F2 V	30	1.5	10.68	…	6.45	5.45
HD 200798	Tuc	45	A5/A6 IV/V	20	2.0	10.68	…	6.69	6.07
GM Tau	τ Aur	140	M6.5	2	…	8.59	…	…	10.63
I0 45251+3016	τ Aur	140	K5	2	…	8.59	…	11.60	8.13
Haro 6-37	τ Aur	140	K6	2	0.8	8.48	CTT	13.42	7.31
VXR 03	IC 2391	155		53	…	7.75	…	10.95	14.86
L36	IC 2391	155	F6V	53	…	7.75	…	9.83	8.63
VXR 31	IC 2391	155		53	…	7.75	…	11.22	9.69
H21	IC 2391	155		53	…	7.75	…	11.69	9.54
SHJM 3	IC 2391	155	K3e	53	0.8	7.75	…	12.63	9.69
L33	IC 2391	155	F5 V	53	…	7.75	…	9.59	8.36
H35	IC 2391	155	F9	53	…	7.75	…	10.34	8.99
CHXR 3	Cham	140	K3	0.5	0.9	7.63	WTT	12.26	7.36
CHXR 10	Cham	140	M0	2	0.9	7.63	CTT	11.69	8.20
ROX 3/V2245 Oph	Ophiuchus	160	M1	2	…	7.51	…	13.12	8.78
HR 6070	β Pic	43	A0 V	20	3.0	7.45	…	4.80	4.74
PreibZinn 9985	U Sco	145	K2	2	0.9	7.13	…	…	8.18

TABLE 3 (*Continued*)

Name	Cluster	Distance (pc)	Spectral Type	Age (Myr)	Star Mass[a] ($M_{\odot}$)	Signal (μas)	T Tauri Class	V (mag)	2MASS K_s (mag)
HR 136	Tuc	45	A0 V	20	3.0	7.12	…	5.07	4.99
HR 9062	Tuc	45	A1 V	20	3.0	7.12	…	5.00	4.82
SHJM 6	IC 2391	155	K0	53	1.0	6.20	…	11.86	9.79
VXR 62	IC 2391	155		53	1.0	6.20	…	11.73	15.03
VXR 67	IC 2391	155		53	1.0	6.20	…	11.71	13.61
VXR 16	IC 2391	155		53	1.1	5.64	…	11.84	14.58
VXR 72	IC 2391	155	G9	53	1.1	5.64	…	11.46	9.59
HR 126	Tuc	45	B9 V	20	4.0	5.34	…	4.36	4.48
TWA 11A	TW Hya	60	A0 V	10	3.0	5.34	…	5.78	5.77

[a] The masses presented here are either taken from the literature or are estimated using the isochrones of D'Antona & Mazzitelli (1994).
[b] Preibisch & Zinnecker (1999).

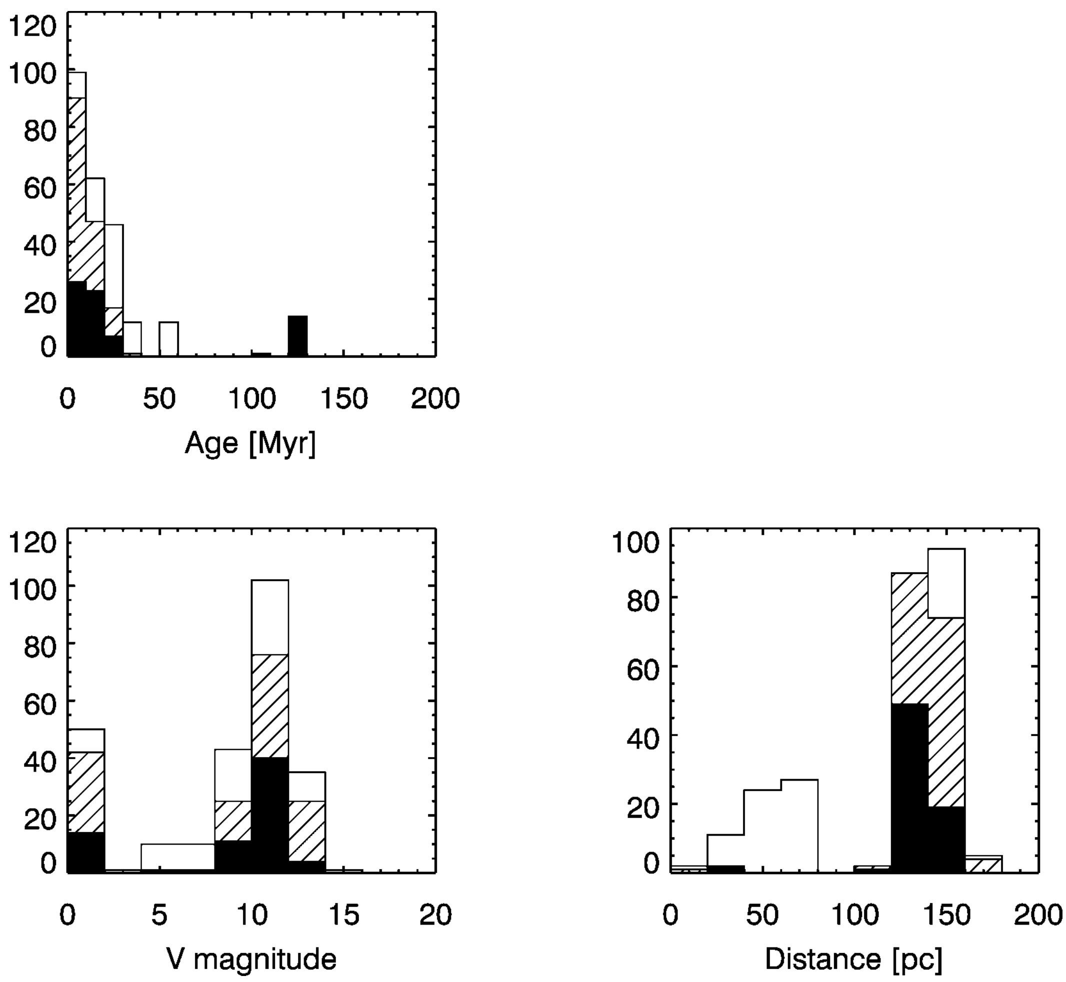

FIG. 2.—Histograms of the properties of the *SIM*-YSO sample. The slashed and black bars show those targets potentially eliminated and remaining, respectively, after cuts from photometry or nearby companions. The white bars represent those targets yet to be observed in the precursor surveys.

TABLE 4
PALOMAR TARGET SAMPLE

Target	V (mag)	2MASS K_s (mag)	Spectral Type	Age (Myr)	Distance (pc)
HII 1032	11.1	9.16 ± 0.02	G8	125	130
HII 1095	11.92	9.67 ± 0.02	K0	125	130
HII 1124	12.12	9.86 ± 0.02	K1	125	130
HII 1136	12.02	12.14 ± 0.02	G8	125	130
HII 1275	11.47	9.53 ± 0.02	G8	125	130
HII 1309	9.58	8.28 ± 0.02	F6	125	130
HII 1514	10.48	8.95 ± 0.02	G5	125	130
HII 1613	9.87	8.57 ± 0.02	F8	125	130
HII 1794	10.2	8.89 ± 0.02	F8	125	130
HII 1797	10.09	15.04 ± 0.11	F9	125	130
HII 1856	10.2	8.66 ± 0.02	F8	125	130
HII 2366	11.53	9.55 ± 0.02	G2	125	130
HII 430	11.4	9.47 ± 0.02	G8	125	130
HII 489	10.38	8.87 ± 0.02	F8	125	130
AA Tau	12.82	8.05 ± 0.02	K7	2	140
BP Tau	11.96	7.74 ± 0.02	K7	2	140
DL Tau	13.55	7.96 ± 0.02	G	2	140
DM Tau	13.78	9.52 ± 0.02	K5	2	140
DN Tau	12.53	8.02 ± 0.02	M0	2	140
DQ Tau	13.66	7.98 ± 0.02	M0	2	140
DR Tau	13.6	6.87 ± 0.02	K5	2	140
GK Tau	12.5	7.47 ± 0.02	K7	2	140
IP Tau	13.04	8.35 ± 0.02	M0	2	140
IQ Tau	14.5	7.78 ± 0.02	M0.5	2	140
IW Tau	12.51	8.28 ± 0.03	K7	2	140
LkCa 19	10.85	8.15 ± 0.02	K0	2	140
V1072 Tau	10.3	8.30 ± 0.02	K1	2	140
V830 Tau	12.21	8.42 ± 0.02	K7	2	140
V836 Tau	13.13	8.60 ± 0.02	K7	2	140

paired together to act as each other's point-spread function (PSF). Two sets of known binary stars with high-quality orbital solutions (WDC 09008+4148 and WDC 23052−0742) were also observed to provide an accurate determination of the plate scale and image orientation. During these observations, each binary was placed in multiple positions over the field of view of the camera.

All the images were sky-subtracted, flat-fielded, and corrected for bad pixels. We used a number of methods for image registration prior to PSF subtraction. The best method involved using the centroid of either the waffle pattern or the "Poisson" spot (Metchev 2006). Using these methods, we were able to achieve a registration accuracy of 2.3 and 0.7 pixels, respectively, which is comparable to the accuracy achieved in a similar survey using the same instrument (Metchev & Hillenbrand 2004). After registration, the median of each image stack was calculated to produce the final image (see Fig. 3). The images of those target stars with similar magnitudes and colors are paired and subtracted to produce a difference image intended to reduce the residual flux within 1″ of the coronagraphic spot. Prior to subtraction, each pair of images was scaled to have the same peak flux within the coronagraph halo to ensure a minimal residual flux after subtraction. Figure 4 shows the

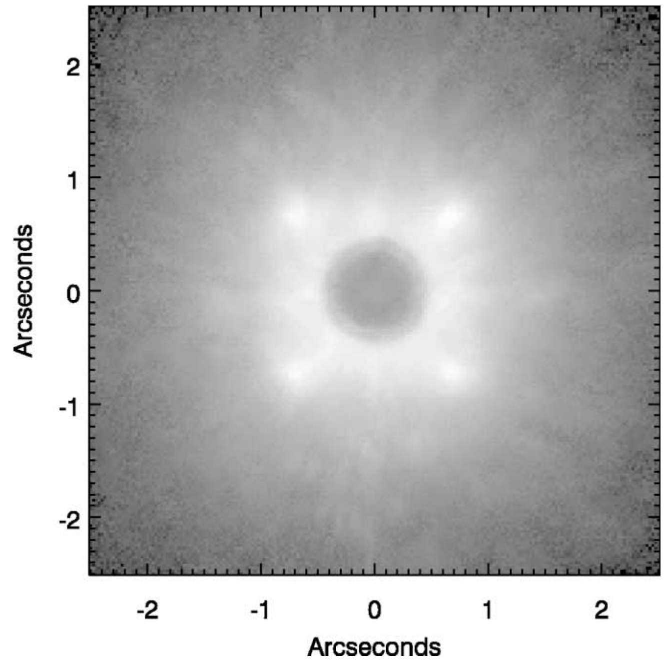

FIG. 3.—Stretched gray-scale image of LkCa 19 highlighting the Poisson spot and waffle pattern inherent in the Palomar AO+coronagraph PSF. North is up and east is to the left.

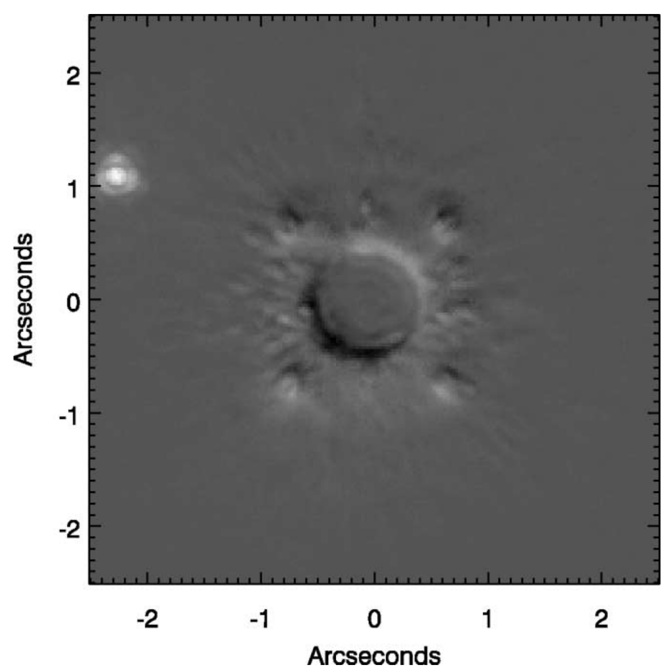

FIG. 4.—Gray-scale difference image of GK Tau and V830 Tau. The apparent companion to GK Tau is 2.4″ away but is most likely a background star, due to its blue colors and non–common proper motion. North is up and east is to the left.

difference image of GK Tau and V830 Tau, with a bright companion candidate next to GK Tau.

A thorough visual inspection of both the median-averaged coronagraphic images and the difference images was performed to identify all potential companions. All visual companions identified in these images are listed in Table 5, along with their distance from the center of the coronagraph, the position angle, and the K_s magnitude. The coronagraphic images have been flux-calibrated using the images taken with the primary star offset from the coronagraph while accounting for a difference in integration time and the well-defined neutral-density filter used for the off-spot images (Metchev & Hillenbrand 2004). The magnitudes for both the primary stars in the off-spot images and the companions in the coronagraphic images are estimated from aperture photometry with an aperture of 0.9″ and a sky annulus of 1.1″–1.4″. The K_s-band magnitudes of the primaries were taken from the Two Micron All Sky Survey (2MASS; Cutri et al. 2003). Since many of the target stars are variable in the optical, the near-infrared photometric calibration may be uncertain, although these stars are typically 2–3 times less variable in the infrared than in the visible (Eiroa et al. 2002).

TABLE 5
VISUAL COMPANIONS TO PLEIADES AND TAURUS TARGETS

Target	Separation (arcsec)	P.A. (deg)	K_s (mag)
HII 1032	12.7	45.0	16.0
HII 1309	11.2	−27.2	15.0
HII 1309	12.1	108.8	15.2
HII 1797	6.6	−8.8	15.7
HII 489	13.4	144.4	17.1
AA Tau	5.9	98.6	15.2
BP Tau	3.1	−83.6	14.0
BP Tau	5.6	8.0	15.0
DL Tau	12.8	22.7	13.4
DL Tau	8.5	61.8	14.5
DL Tau	16.7	134.8	14.8
DL Tau	11.9	15.0	15.4
DQ Tau	7.3	149.6	15.3
GI Tau	8.3	1.7	14.6
GK Tau	2.4	62.1	12.1
IP Tau	3.7	124.3	15.1
IQ Tau	9.8	165.5	14.9
IQ Tau	13.9	−64.6	15.3
IQ Tau	10.7	−35.9	13.4
IQ Tau	10.2	−33.9	13.6
LkCa 19	4.3	−77.4	16.2
LkCa 19	11.8	−36.2	13.9
V830 Tau	7.1	−52.3	17.0
V830 Tau	11.2	58.3	15.8
V830 Tau	11.8	100.3	17.5
V830 Tau	7.8	146.1	17.7

3.2. Results

In Taurus and the Pleiades, 10 out of 16 of the targets (63%) and 5 out of 14 (36%), respectively, have visual companions within the 25″ (∼1750 AU) field of view. Almost all of the companions lie >2″ away from the target, corresponding to a distance greater than 300 AU. To estimate the sensitivities of our images as a function of distance from the star, we employ "PSF planting," in which a PSF corresponding to an object of known brightness is inserted into the image to determine whether it is detectable. A PSF extracted from the off-spot image of each target is sky-subtracted, normalized, multiplied by an array of contrast values ($\Delta K_s = 7.7$–15.1 mag), and placed at a range (0″–5″) of distances from the target at random position angles. We completed 10,000 iterations of the PSF-planting algorithm to fill out the parameter space of contrast and distance from the primary star. To determine whether the planted star is detected, the image is cross-correlated with a flux-normalized PSF. The correlation values are binned according to the distance of the PSF from the star, in increments of 0.1″. For each distance bin, we estimate the minimum PSF intensities that resulted in a correlation value of 0.9 or higher. The intensities are converted into magnitudes using the flux calibration from the off-spot image and the 2MASS K_s magnitude of the star. Figure 5 plots the largest K_s magnitude difference between the target star and planted PSF with a correlation of 0.9 as a function of distance from the star for all targets with calibration data. Table 6 lists the values of the faintest detectable K_s magnitudes at 0.5″, 1″, 2″, 5″, and 9″. On average, we were able to detect sources with a magnitude contrast of $\Delta K_s = 4$–7 mag at 2″ and $\Delta K_s \sim 8$–10 at 5″. The range of image contrasts is due primarily to variations in seeing conditions throughout the night, since all the targets had similar magnitudes and integration times.

Calibration binaries were used to estimate the plate scale of the PHARO camera. For the 2004 October data, we adopt a plate scale of 25.11 ± 0.04 mas pixel^{-1}, estimated from three different binary stars (WDS 09006+4147, WDS 18055+0230, and WDS 20467+1607) that were observed very close to our observations, using the same instrument (2004 October 4–5; Metchev 2006). For the 2005 data, we estimate a plate scale of 25.21 ± 0.36 mas pixel^{-1}. This plate scale and its uncertainty comes from the average and standard deviation of the separation of one binary (WDS 09006+4147) placed in multiple positions across the field of view after correction for the known distortion in the camera.

To estimate the position of the occulted target star in these images, we use the waffle pattern inherent to every PSF (see Fig. 3). Each waffle pattern consists of four points in a box pattern around the star. The center of the coronagraphic PSF is determined from the intersection of the two diagonal lines fitted to the centroid positions of the four peaks in the waffle pattern. Using this method, we are able to determine the position of the star to within 0.35 pixels, estimated from the standard deviation of the stellar position in a stack of subframes.

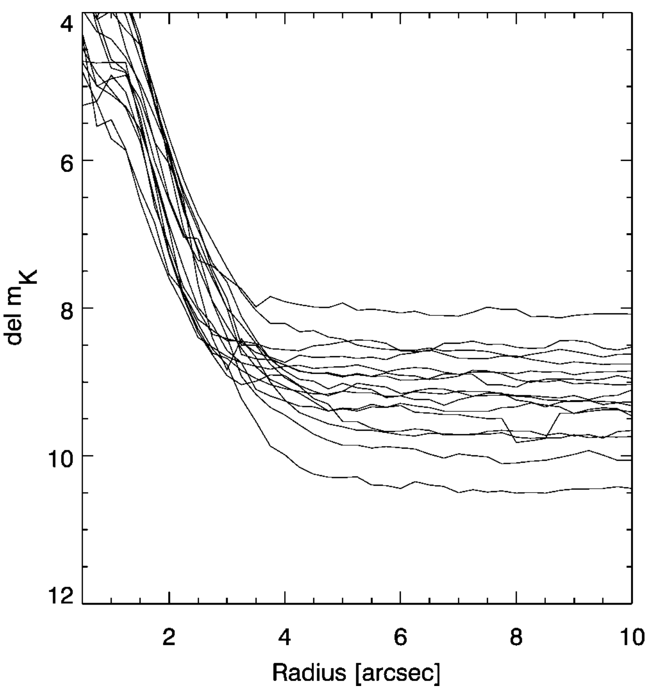

FIG. 5.—Plot of the contrast in ΔK_s magnitude detectable in the PHARO images as a function of separation from the target.

TABLE 6
PALOMAR IMAGING SENSITIVITIES (K_s MAGNITUDE)

Target	T_{int} (s)	0.5″	1″	2″	5″	9″
HII 1032	1200	12.84	13.55	15.91	18.01	18.17
HII 1136	1200	14.26	14.99	16.74	17.86	17.65
HII 1797	1200	12.17	12.04	14.53	17.19	17.28
HII 1794	1200	12.18	12.53	14.70	17.78	17.87
HII 489	1200	14.68	13.93	16.20	17.57	17.76
AA Tau	1200	13.31	11.44	15.20	17.16	17.36
BP Tau	1200	11.08	11.65	14.26	17.41	17.57
CI Tau	1200	12.02	12.10	13.68	17.67	17.67
DL Tau	1200	12.51	13.17	15.24	17.22	17.20
DN Tau	900	12.80	10.91	14.13	17.13	17.18
DQ Tau	1200	12.84	13.24	15.01	17.49	17.39
GK Tau	1200	11.58	11.22	12.90	16.94	17.15
GI Tau	1200	12.00	12.25	14.16	17.26	17.34
IP Tau	1200	13.86	13.00	15.78	17.04	17.11
IQ Tau	1200	12.27	13.18	14.93	16.82	16.93
LkCa 19	900	12.46	12.55	14.93	17.97	18.22
V830 Tau	1200	13.59	14.85	17.09	20.15	20.36

The positions of the companion candidates are estimated from their centroids and have errors of 0.5–1 pixel, depending on the brightness of the companion, seeing conditions, and telescope drift. The pixel positions for all primaries and their companions are corrected for the distortion determined for the PHARO camera (Metchev 2006). The errors in the stellar position and PHARO pixel scale are propagated into the error of the offsets of the companion candidates from their primaries.

Figure 6 plots the offset in R.A. and decl. of companion candidates to BP Tau, IP Tau, GK Tau, and LkCa 19. These four sources all have objects within at least 4.5″ (675 AU). While the probability of these companion candidates being background sources goes up with their separation from the target star, the discovery of a number of brown dwarf companions at wide separations (>200 AU) makes these companion candidates worth investigating further. The crosses denote the positional offsets at the observing epochs of the Palomar data (2004, 2005), in addition to data taken from *Hubble Space Telescope* (*HST*) WFPC2 and NICMOS data when available. The *HST* data were collected in 1999 as part of a program to detect faint debris disks (Krist et al. 2000) and therefore provide a long time baseline for the determination of common proper motion. In most cases, the target star in the WFPC2 data is saturated, and the position of the star is estimated from the intersection of the diffraction spikes. The size of the crosses denotes the 3 σ positional uncertainties (1 $\sigma \sim 12$ mas for the Palomar data, and 1 $\sigma \sim 3$ mas for the WFPC2 data; J. Krist 2006, private communication). The curvy solid lines depict the changes in the offsets expected if the companion were a stationary background object. The dotted lines represent the errors in the published proper motions (Frink et al. 1997). If the companions are associated with the target stars, the offsets will coincide with one another at all epochs, since the objects will share the same space motions. Table 7 lists the reduced χ^2 values estimated from the positional data and uncertainties. Two hypotheses are tested: common proper motion and non–common proper motion. In the first scenario, the χ^2 is derived from the assumption that all the data points should lie on top of the first epoch (1999) data point. For the second scenario, the χ^2 is derived from the assumption that the data points should lie on the vector produced by the change in the offset between the science target and stationary background star. The uncertainties for this case include both the positional uncertainties and the uncertainty in the proper motion of the T Tauri star (Frink et al. 1997). An unmodeled source of uncertainty that may inflate the χ^2 values in the second scenario is the unknown proper motion of the companions. Based on this analysis, we conclude that there is evidence for common proper motion for the companion to GK Tau, evidence for non–common proper motion for the companion to BP Tau, and ambiguous evidence for either scenario for IP Tau and LkCa 19. These last two sources would benefit from more accurate positional data and a longer time baseline. If the GK Tau companion is truly a physical companion, then based on its K_s magnitude, it would be roughly a M2–3 star with a mass of ~0.5 $M_\odot$.

We have begun a similar high-contrast imaging survey of the *SIM*-YSO targets in the Upper Sco subgroup of the Sco-Cen association (1–2 Myr, 145 pc), using the NAOS-CONICA (NACO) camera on the VLT. The NACO camera has been used to discover a number of low-mass companions, including 2MASSW J1207334−393254 and GQ Lupi (Neuhäuser et al. 2005; Chauvin et al. 2005). It has a pixel scale of 27 mas

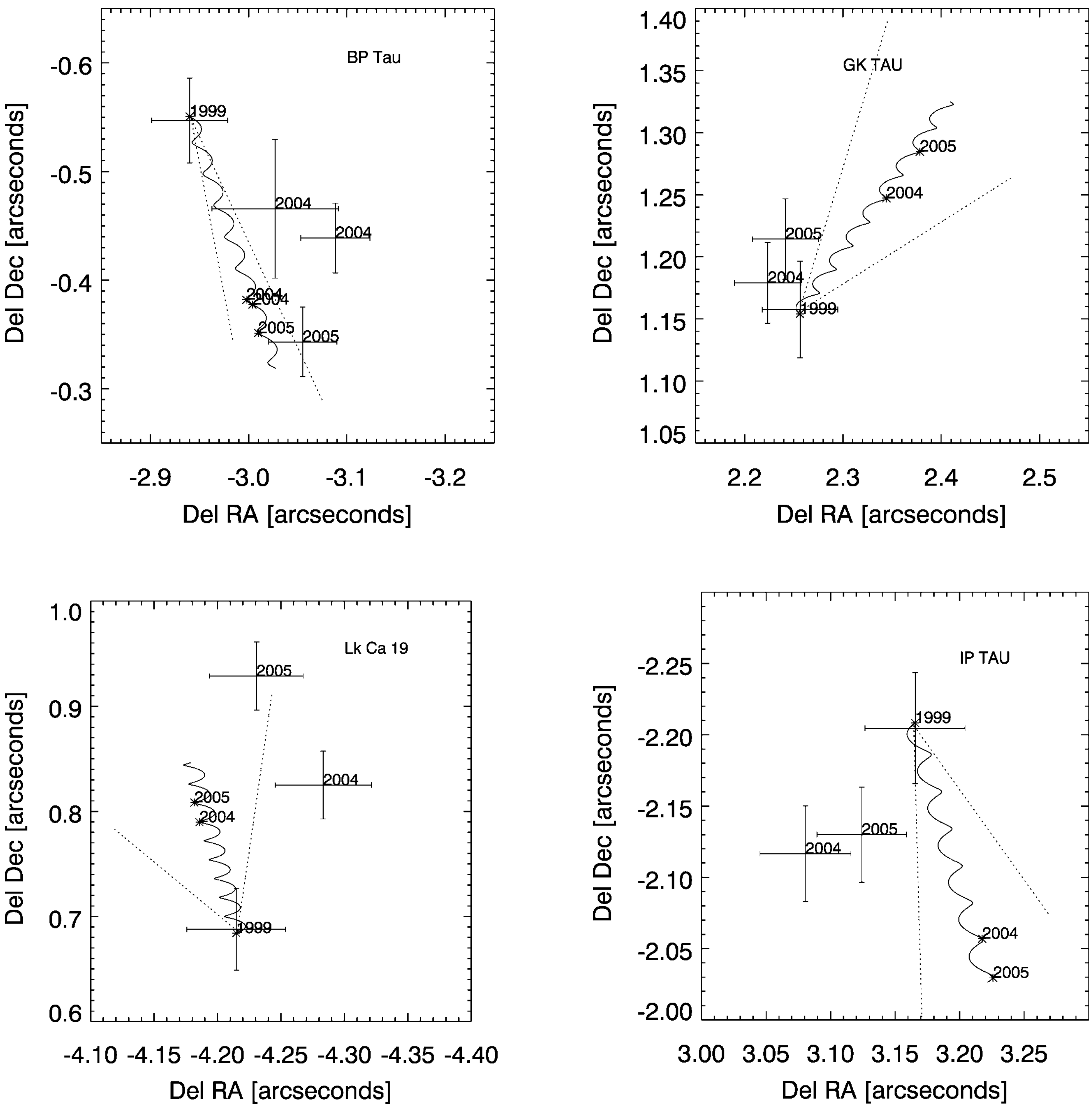

FIG. 6.—Plot of the offset in R.A. and decl. between BP Tau, GK Tau, IP Tau, and LkCa 19 and their companion candidates. The WFPC2 data point taken in 1999 January is used as the initial data point. Each measured offset is noted with a cross and an epoch label. The curvy solid line shows the expected motion of the star, assuming measured proper motions from Frink et al. (1997). The expected offset of the companion if it were a steady background object is labeled on the proper motion curve, with epoch values (2004, 2005). Table 6 lists the reduced χ^2 values associated with fits to the data points, which assume the companion candidates has common and non–common proper motion with their primary stars.

TABLE 7
Reduced χ^2 Values from Common and Non–common Proper Motion Fits

Target	Reduced $\chi^2_{\mathrm{Common\ PM}}$	Reduced $\chi^2_{\mathrm{Non-common\ PM}}$
BP Tau	26	2.5
GK Tau	1.4	4.1
IP Tau	4.2	4.4
LkCa 19	43	6.3

pixel^{-1} and a field of view (FOV) of 28″, with the potential of achieving ΔK_s sensitivities of 10 at 1″ (Chauvin et al. 2004). So far, we have collected data on 20 targets, with a number of them having companion candidates within 1″. We will collect second-epoch observations for these sources at a later date.

3.3. Comparison to Other Surveys

There have been a few other ground AO and space-based surveys for low-mass companions to young stars (1–200 Myr) that have found a few brown dwarfs with separations between 75 and 1000 AU. These surveys had sample sizes ranging from 30 to 100 targets, with two surveys finding two to three brown dwarfs when targeting stars in nearby associations (Metchev 2006; Lowrance et al. 2005), and one survey finding no brown dwarfs when targeting X-ray–selected T Tauri stars in the Chamaeleon and Sco-Cen OB associations (Brandner et al. 2000). Metchev (2006) has estimated a completeness-corrected percentage of brown dwarfs at ~7% ± 3% (1 σ confidence) around F5–K5 stars with an age and separation range of 3–500 Myr and 30–1600 AU, respectively. Therefore, our finding of no very low-mass objects in a survey of 30 stars is consistent with previous programs, given the stated uncertainties. Whether there is a significant dearth of brown dwarfs or planetary-mass objects around young stars still requires a larger sample of targets with similar sensitivities to allow for a direct comparison of detection statistics.

Stellar multiplicity surveys of star formation regions such as Taurus and the Pleiades have revealed binary companion fractions of 60% (over 20–500 AU) and 30% (over 1–900 AU), respectively (Ghez et al. 1993; Bouvier et al. 1997). However, we used these and other surveys mentioned previously (see § 2) to remove stars with stellar companions within 2″ in defining our initial sample. Thus, it is not surprising that our survey did not add to the statistics for stellar multiplicity in these clusters.

3.4. Speckle Imaging and Additional AO Imaging of the Taurus Sample

To complement the adaptive optics survey at Palomar, a number of the targets in the sample have been observed using high-resolution imaging techniques at the Keck Observatory. The purpose of this project was to look for companions at separations too close to be resolved at Palomar, and too wide to be detected via spectroscopic techniques. A summary of the results of this portion of the project is given in Table 8.

In total, 17 objects in Taurus, TW Hydrae, or AB Doradus were surveyed at Keck. Three of these were imaged using speckle interferometry at the K band (2.2 μm) on Keck I, and 14 were observed using adaptive optics and the K' (2.3 μm) or L' band (3.5 μm) on Keck II. The dates of these observations are given in Table 8, along with the total exposure time on each target. For details on the data reduction and analysis of both the speckle and the AO data taken at Keck, please see Konopacky et al. (2007).

For all 17 sources, no companions were found to within 0.05″. For each source, we estimated our sensitivity to companions by finding the limiting detectable flux ratio with respect

TABLE 8
Keck Imaging Sensitivities

Object	Date of Obs.	Method (Sp. or AO)	Total Exp. Int. Time (s)	ΔK Limit 0.05″	ΔK Limit 0.1″	ΔK Limit ≥0.5″	Mass Limit ($M_\odot$) 0.05″	Band
TWA 23	2005 May 27	Sp.	78.1	2.9	3.7	6.9	0.10	K
TYC 7660-0283	2005 May 27	Sp.	78.1	3.9	4.1	6.5	0.08	K
GM Tau	1997 Oct 12	Sp.	156.2	3.9	3.9	6.5	≲0.02	K
Anon 1	2005 Dec 12	AO	120	3.8	4.4	6.2	0.06	K
BP Tau	2005 Dec 12	AO	120	5.5	4.3	6.2	0.03	K
DG Tau	2005 Dec 12	AO	120	5.8	3.5	5.9	0.02	K
HD 283572	2005 Dec 12	AO	54.3	4.6	4.8	6.3	0.03	K
IP Tau	2005 Dec 12	AO	120	3.7	4.5	5.3	0.06	K
IQ Tau	2005 Dec 12	AO	120	5.0	4.7	5.9	0.03	K
V1072 Tau	2005 Dec 12	AO	120	5.1	5.5	6.5	0.03	K
DN Tau	2005 Dec 12	AO	120	4.7	5.1	6.2	0.03	K
V830 Tau	2005 Dec 12	AO	60	2.9	3.9	5.8	0.15	K
DR Tau	2005 Dec 12	AO	54.3	3.4	3.9	6.6	0.14	K
HIP 113579	2005 Jul 16	AO	3.0	3.7	3.5	5.7	0.24	L
HIP 113597	2005 Jul 16	AO	6.0	3.0	5.1	5.7	0.12	L
HIP 114066	2005 Jul 16	AO	6.0	2.9	3.0	5.3	0.09	L
HIP 115162	2005 Jul 16	AO	6.0	3.0	4.9	5.2	0.39	L

TABLE 9
Keck Interferometry Results

Target	K Mag.	No. of Ints.	Avg. V^2	Avg. σ	Calibrators
DN Tau	8.0	1	1.02	0.09	HD 283444, HD 283886
V830 Tau[a]	8.4	1	0.85	0.10	HD 283668, HD 282230, HD 29334
V830 Tau[b]	8.4	1	0.89	0.07	HD 283668, HD 282230, HD 29334
V830 Tau	8.4	1	1.08	0.13	HD 283444, HD 283886
V1171 Tau	9.2	2	0.98	0.05	HD 24132, HD 23289, HD 284316
V1072 Tau	8.3	1	1.13	0.10	HIP 19757, HD 285816
V1075 Tau	8.9	1	1.08	0.10	HIP 19757, HD 285816
HD 282973	8.6	2	0.97	0.06	HD 24132, HD 23289, HD 284316
HD 282971	8.7	2	0.99	0.06	HD 24132, HD 23289, HD 284316
HD 23584	8.3	2	0.98	0.06	HD 24132, HD 23289, HD 284316

[a] Observation from 2003 October 16.
[b] Observation from 2004 January 7.

to the source as a function of radius, and then using the models of Baraffe et al. (1998; $\alpha = 1.0$) to convert these flux ratio limits into mass limits for the closest radius bin of 0.5″. In general, the speckle measurements probe regions closer than 0.05″ with much greater sensitivity than AO, but given the combination of the two techniques for this survey, we cut off our official completeness at 0.5″. We plan to observe the remaining targets visible from the Northern Hemisphere with either Keck AO or speckle imaging and are beginning a survey of the targets in the Southern Hemisphere using Lucky imaging, a similar observational technique at optical wavelengths (Law et al. 2006).

4. INTERFEROMETRIC OBSERVATIONS OF STARS IN TAURUS AND THE PLEIADES

The Keck Interferometer (KI) was used to make near-infrared, long-baseline interferometry observations of three sources in the Pleiades and five sources in Taurus. These observations are part of a long-term program to study the multiplicity fraction of these sources. In particular, the interferometer is sensitive to companions within 30 mas of the primary star and having a K magnitude difference of 3 mag or less.

The observations were taken on 2006 November 10, with KI configured in the five-channel K band (2.18 μm central wavelength) mode described in Colavita et al. (2003). Calibrators were chosen to match the targets in K magnitude and were reduced with the standard parameters (Colavita et al. 2003), including the ratio correction for imbalanced flux on the two paths of the interferometer. The calibrator sizes were all set to a 0.1 ± 0.05 mas diameter, but in all cases, the calibrator diameter did not contribute significantly to the final uncertainty. The primary KI data product is the normalized visibility amplitude squared, for which a value of 1 indicates an unresolved source. The uncertainty given is the quadrature combination of the scatter in the target measurement and the uncertainty in the system visibility (which in this case is dominated by the scatter in the calibrator measurements). Table 9 lists the targets, the number of integrations, the calibrated visibility and total uncertainty, and the calibrators used for each target. The uncertainty varies, due to the number of integrations and the difficulty in observing sources with fainter V magnitudes.

All targets observed in this sample, except V830 Tau, are unresolved; i.e., they are consistent with a point source at this resolution. At the distance to Taurus or the Pleiades, the central star will be unresolved (<0.1 mas). Using the best uncertainties of 0.06, we can place limits on the size of the emission, of 1.3 mas (1.8 AU) in diameter (3 σ) for a uniform disk, or on the presence of overresolved (diffuse) emission within the 50 mas FOV, of <10% (3 σ). Additional observational epochs are needed to constrain the multiplicity. V830 Tau has visibilities estimated from earlier epochs of data (2003, 2004; Akeson et al. 2005), which differ from the expected value for an unresolved source by a few σ (see Table 9). Future observations of this star with KI are planned in order to determine the nature of the resolved emission.

5. RADIAL VELOCITY VETTING

Some of the target stars will have stellar or substellar companions that are not detectable by direct imaging (separations <50 AU). We are conducting a number of radial velocity (RV) surveys of potential *SIM*-YSO stars to determine whether the targets have unseen companions that might complicate the astrometric detection of planetary-mass objects. For example, a $20M_J$ companion in a 1 yr orbit around a 0.8 $M_\odot$ star has an RV amplitude of 660 m s^{-1}. At 140 pc, this object would produce an astrometric signature of 160 μas that would swamp the signal from any lower mass planets. Located just a few milliarcseconds from its parent star, the brown dwarf companion would be undetectable by direct noninterferometric imaging. The goal of the RV program is to achieve accuracies on the order of <500 m s^{-1} over 3–4 years, depending on the $v \sin i$ and photospheric instabilities of each star, with the goal of achieving limits on stellar and substellar companions on orbits interior of 5 AU.

There are two radial velocity surveys presently being conducted on the *SIM*-YSO targets in both the Northern and Southern Hemispheres. The southern survey was begun in 2003 July using the echelle spectrograph ($R = 25{,}000$) on the CTIO

TABLE 10
$v \sin i$ VALUES FOR SCO-CEN TARGETS

Target	$v \sin i$ (km s^{-1})	Target	$v \sin i$ (km s^{-1})
TYC 8648-446-1	10	TYC 8238-1462-1	25
TYC 8283-264-1	10	TYC 8654-1115-1	25
TYC 8282-516-1	13	TYC 8655-149-1	25
TYC 8645-1339-1	15	TYC 9245-617-1	25
TYC 9246-971-1	15	TYC 7833-2559-1	25
TYC 7796-1788-1	15	TYC 8295-1530-1	25
TYC 9244-814-1	15	TYC 7353-2640-1	25
TYC 7319-749-1	15	TYC 8636-2515-1	30
TYC 8317-551-1	15	TYC 8646-166-1	30
TYC 8242-1324-1	18	TYC 7310-2431-1	30
TYC 8249-52-1	18	TYC 8294-2230-1	30
TYC 8259-689-1	18	TYC 7824-1291-1	33
TYC 8297-1613-1	18	TYC 8652-1791-1	35
TYC 7848-1659-1	18	TYC 7852-51-1	40
TYC 8640-2515-1	20	TYC 8633-508-1	45
TYC 8644-340-1	20	TYC 8248-539-1	50
TYC 7811-2909-1	20	TYC 7333-1260-1	55
TYC 8667-283-1	23	TYC 7851-1-1	55
TYC 7822-158-1	23	TYC 7783-1908-1	63
TYC 9212-2011-1	25	TYC 8270-2015-1	65

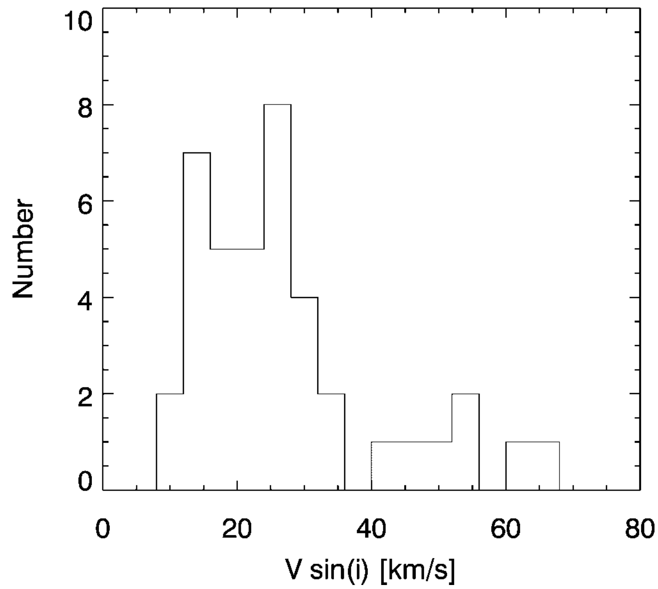

FIG. 7.—Histograms of the values of $v \sin i$ estimated from the Sco-Cen sample.

4 m telescope (PI: S. Mohanty). All 42 of the targets in this survey were in the Sco-Cen association. Only one epoch of these targets has been collected to date, because of the unfortunate retirement of this instrument on this telescope. Many of the stars in Sco-Cen turned out to be fast rotators (>10 km s^{-1}; see Table 10 and Fig. 7), which is not surprising, since at 10–20 Myr of age, there is ample time for the stars to spin-up due to stellar contraction.

The northern survey began in 2004 October and used the coudé echelle spectrograph ($R = 60{,}000$) on the 2.7 m Harlan J. Smith Telescope at McDonald Observatory (PI: L. Prato). Survey targets are located in the Pleiades and in the Taurus star-forming region. To date, 51 objects have been observed at multiple epochs, with an RV precision of 140 m s^{-1}. This survey makes use of simultaneous *BVR* photometry to search for correlations between RV periods and rotation that are indicative of starspot modulation rather than the presence of a low-mass companion. Initial results that include a few targets with potential companions or signs of starspots will be presented in a forthcoming publication (M. Huerta et al. 2007, in preparation; Huerta et al. 2005).

6. PHOTOMETRIC MONITORING

The photospheric activity that affects radial velocity and transit measurements affects astrometric measurements as well, but as we now show, at levels consistent with the secure detection of gas giant planets using *SIM*. From measurements of photometric variability (Herbst et al. 1994; Bouvier & Bertout 1989; Bouvier et al. 1995) plus Doppler imaging (Strassmeier & Rice 1998), T Tauri stars are known to have active photospheres, with large starspots covering significant portions of their surfaces (Schuessler et al. 1996), as well as hot spots due to infalling accreting material (Mekkaden 1998). Day-to-day changes arise primarily because of rotation, whereas month-to-month variations reflect changes in the spot sizes and their distribution across the surface. Long-term monitoring is essential, because different stars have different levels of magnetic activity, and these levels can change with time. These effects can produce large photometric variations, which can significantly shift the photocenter of a star. In the simplest approximation, a completely black starspot covering a small fraction ($\beta \ll 1$) of a stellar hemisphere will shift the photocenter by an angle

$$\Delta\phi(\theta) \sim \beta \sin\theta \cos\theta \frac{R_\star}{D_\star}$$
$$= 33.4\beta \frac{R_\star}{R_\odot} \frac{140 \text{ pc}}{D_{\text{pc}}} \sin\theta \cos\theta \ \mu\text{as}, \quad (2)$$

where $R_\star$ is the stellar radius, D_* is the distance to the star, and θ is the longitude of the starspot relative to the line of sight. We have assumed that the spot is on the star's equator and that the star is observed edge-on relative to its rotation axis. The shift in the photocenter $\Delta\phi(\theta)$ will increase as the spot rotates away from a face-on longitude ($\propto \sin\theta$), following the rotation of the star as the spot shrinks in projected area ($\propto \cos\theta$) and eventually goes behind the star. Relative to the fractional change in stellar brightness, $\Delta I/I(\theta) = \beta\cos\theta$, and averaging over $-\pi/2 < \theta < \pi/2$, we get an rms dispersion in the location of the photocenter (the "astrometric jitter"), given by

$$\langle \Delta\phi \rangle = \alpha \left\langle \frac{\Delta I}{I} \right\rangle \frac{R_\star}{D_\star}$$

$$= 1.8 \frac{R_\star}{R_\odot} \frac{140 \text{ pc}}{D_{\text{pc}}} \frac{\Delta R(\text{mag})}{0.05 \text{ mag}} \ \mu\text{as}, \qquad (3)$$

where α is a geometric term of order 1.1. A more careful analysis takes into account the fact that the spots are not completely black, but rather that they emit with a temperature ~1000 K cooler than the photosphere and are located over a range of typically high latitudes, and that an ensemble of stars will be observed at random angles to the line of sight. A Monte Carlo simulation shows a linear relationship like that of equation (3), but with a smaller coefficient:

$$\langle \Delta\phi(\text{Monte Carlo}) \rangle = 0.9 \frac{R_\star}{R_\odot} \frac{140 \text{ pc}}{D_{\text{pc}}} \frac{\Delta R(\text{mag})}{0.05 \text{ mag}} \ \mu\text{as}. \qquad (4)$$

For a typical T Tauri star radius of 3 $R_\odot$ in Taurus, we see that the astrometric jitter is less than 3 μas for *R*-band variability less than or equal to 0.05 mag (1 σ). Thus, the search for Jovian planets with astrometric amplitudes greater than 6 μas is possible for stars less variable than about 0.05 mag in the visible, even without a correction for jitter that may be possible using astrometric information at multiple wavelengths. Other astrophysical noise sources, such as offsets induced by the presence of nebulosity and stellar motions due to disk-induced nonaxisymmetric forces, are negligible for appropriately selected stars. Finally, it is worth noting that searching for terrestrial planets will be difficult until stars reach an age such that their photometric variability falls well below 0.01 mag and the corresponding astrometric jitter falls below 1 μas. Even then, color-dependent astrometric corrections may be needed for the most sensitive measurements.

Since young stars have active photospheres, it is important that we assess the degree of photospheric activity to determine the best targets for the program. The *SIM*-YSO team has two separate programs conducting photometric monitoring of the sample targets in the Northern and Southern Hemispheres. The southern targets are being observed in the *R* band (0.9 μm) at CTIO, using the SMARTS (Small and Moderate Aperture Research Telescope System) program (PI: M. Simon), which is composed of small (0.9–1.5 m) telescopes in the Southern Hemisphere. To date, they have observed 132 stars in the Sco-Cen and Upper Sco associations. Figure 8 plots the *R* magnitudes of AA Tau and DN Tau taken with the SMARTS survey. The standard deviations of the photometry for these two sources are 0.17 and 1.5, respectively, making the latter source a problematic *SIM*-YSO target.

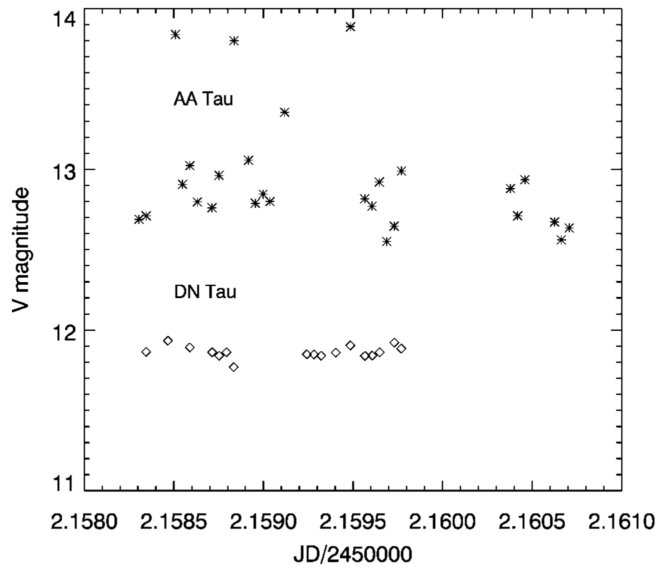

FIG. 8.—Plot of the *V*-band photometry taken for AA Tau and DN Tau. The standard deviations of the photometry for these two sources is 1.5 and 0.17 mag, respectively, making the first source a problematic *SIM*-YSO target.

The northern component of the *SIM*-YSO sample, which includes stars in Taurus and the Pleiades, has been monitored photometrically with small telescopes at the Maidanak Observatory (PI: W. Herbst; Grankin et al. 2007). Approximately 10 data points are obtained on each star during each season to sample the range of variability. The data are taken primarily in the *B*, *V*, and *R* bands, with a small amount taken in the *U* band. Forty-two stars are on the program, and about 450 individual measurements have been obtained each season.

Out of those targets observed to date in both the northern and southern samples, 33% of them have photometric variability that produces astrometric noise greater than 3 μas (or roughly 1 $\sigma \sim$ 0.05 mag) in either the *V* or *R* band (see Table 11 and Fig. 9). Simultaneous monitoring of the variable stars both photometrically and with radial velocity measurements during the *SIM* observations might allow us to model the jitter and derive accurate astrometry. Those targets exhibiting significant amounts of photometric variability will be monitored further to assess whether they should remain in the target list or be relegated to wide-angle observations, which will be sensitive to Jupiter-mass planets farther than 1 AU from the star.

7. DISCUSSION

Through a series of precursor programs to observe all of the stars in the *SIM*-YSO target list, it becomes clear that the ob-

TABLE 11
Stellar Variabilities

Target	Peak to Peak	$\sigma_{\text{st. dev.}}$	Program	Target	Peak to Peak	$\sigma_{\text{st. dev.}}$	Program
HII 1215	0.024	0.009	Maidanak	PreibZinn 9968	0.140	0.045	SMARTS
51 Eri	0.019	0.010	Maidanak	TYC 7326-928-1	0.140	0.045	SMARTS
GJ 3305	0.020	0.010	Maidanak	HD 30709	0.150	0.045	Maidanak
HII 996	0.030	0.010	Maidanak	TYC 8238-1462-1	0.150	0.045	SMARTS
HII 489	0.029	0.012	Maidanak	CHXR 65	0.170	0.045	SMARTS
HII 1309	0.037	0.013	Maidanak	DM Tau	0.136	0.046	Maidanak
CHXR 11	0.040	0.013	SMARTS	PreibZinn 9959	0.140	0.046	SMARTS
HD 141569	0.056	0.013	Maidanak	TYC 7319-749-1	0.180	0.046	SMARTS
HII 1207	0.034	0.014	Maidanak	PreibZinn 9961	0.140	0.047	SMARTS
HII 1797	0.044	0.014	Maidanak	PreibZinn 991	0.140	0.047	SMARTS
HII 1856	0.051	0.014	Maidanak	PreibZinn 9929	0.170	0.047	SMARTS
HII 1095	0.050	0.015	Maidanak	PreibZinn 9937	0.140	0.048	SMARTS
HII 1613	0.054	0.015	Maidanak	TYC 8655-149-1	0.140	0.048	SMARTS
HD 140374	0.060	0.015	SMARTS	TYC 7853-227-1	0.140	0.048	SMARTS
HII 2366	0.041	0.016	Maidanak	PreibZinn 9932	0.130	0.049	SMARTS
PreibZinn 9969	0.050	0.016	SMARTS	TYC 8283-264-1	0.150	0.049	SMARTS
HII 1794	0.055	0.016	Maidanak	HD 149735	0.130	0.050	SMARTS
TYC 9244-814-1	0.050	0.017	SMARTS	TYC 7840-1280-1	0.170	0.051	SMARTS
TYC 8259-689-1	0.060	0.017	SMARTS	TYC 7842-250-1	0.130	0.052	SMARTS
HII 430	0.048	0.018	Maidanak	TYC 8644-340-1	0.130	0.052	SMARTS
TYC 8270-2015-1	0.050	0.018	SMARTS	TYC 8694-1685-1	0.150	0.052	SMARTS
HII 1275	0.056	0.018	Maidanak	PreibZinn 9976	0.160	0.052	SMARTS
TYC 7871-1282-1	0.070	0.018	SMARTS	TYC 7833-2037-1	0.800	0.052	SMARTS
HII 1514	0.059	0.019	Maidanak	TYC 7852-51-1	0.140	0.053	SMARTS
HD 149551	0.060	0.019	SMARTS	PreibZinn 9926	0.170	0.054	SMARTS
PreibZinn 9974	0.060	0.019	SMARTS	PreibZinn 9916	0.170	0.055	SMARTS
TYC 8646-166-1	0.070	0.019	SMARTS	PreibZinn 9984	0.170	0.055	SMARTS
PreibZinn 9 10	0.070	0.019	SMARTS	PreibZinn 9986	0.190	0.056	SMARTS
TYC 7848-1659-1	0.060	0.020	SMARTS	TYC 7824-1291-1	0.190	0.057	SMARTS
CHXR 37	0.070	0.020	SMARTS	PreibZinn 9923	0.150	0.058	SMARTS
CHXR 8	0.070	0.020	SMARTS	TYC 8249-52-1	0.150	0.058	SMARTS
PreibZinn 9919	0.070	0.021	SMARTS	TYC 8645-1339-1	0.170	0.058	SMARTS
TYC 7353-2640-1	0.080	0.021	SMARTS	HD 108611	0.180	0.058	SMARTS
RECX 5	0.090	0.021	SMARTS	TYC 7811-2909-1	0.150	0.062	SMARTS
TYC 9245-617-1	0.060	0.022	SMARTS	TYC 9212-2011-1	0.160	0.062	SMARTS
PreibZinn 9975	0.070	0.022	SMARTS	ROX 3	0.180	0.062	SMARTS
TYC 7828-2913-1	0.070	0.022	SMARTS	V1121 Oph	0.270	0.063	SMARTS
PreibZinn 9964	0.070	0.022	SMARTS	TYC 7815-2029-1	0.220	0.064	SMARTS
TYC 8633-508-1	0.080	0.022	SMARTS	TYC 7858-830-1	0.170	0.065	SMARTS
TYC 8636-2515-1	0.090	0.022	SMARTS	PreibZinn 996	0.190	0.065	SMARTS
PreibZinn 9981	0.080	0.023	SMARTS	PreibZinn 9963	0.200	0.066	SMARTS
HII 1032	0.068	0.024	Maidanak	TAP 35	0.308	0.066	Maidanak
TYC 7310-2431-1	0.080	0.024	SMARTS	TYC 7796-1788-1	0.170	0.067	SMARTS
TYC 8283-2795-1	0.080	0.024	SMARTS	PreibZinn 9940	0.180	0.067	SMARTS
TYC 8667-283-1	0.090	0.024	SMARTS	RECX 4	0.200	0.067	SMARTS
TYC 7305-380-1	0.090	0.025	SMARTS	PreibZinn 9977	0.160	0.068	SMARTS
TYC 7349-2191-1	0.090	0.025	SMARTS	PreibZinn 993	0.200	0.068	SMARTS
TYC 7310-503-1	0.080	0.026	SMARTS	CHXR 18N	0.210	0.068	SMARTS
PreibZinn 9966	0.080	0.027	SMARTS	SR4	0.200	0.069	SMARTS
PreibZinn 9982	0.080	0.027	SMARTS	TYC 7333-719-1	0.240	0.069	SMARTS
TYC 8297-1613-1	0.100	0.027	SMARTS	ROX 43A	0.180	0.072	SMARTS
TYC 9231-1566-1	0.100	0.027	SMARTS	Haro 6-37	0.230	0.075	SMARTS
PreibZinn 992	0.090	0.028	SMARTS	CHXR 66	0.220	0.076	SMARTS
TYC 8258-1878-1	0.090	0.028	SMARTS	PreibZinn 9918	0.240	0.077	SMARTS
TYC 8317-551-1	0.100	0.028	SMARTS	PreibZinn 9955	0.230	0.078	SMARTS
TYC 8652-1791-1	0.100	0.029	SMARTS	V830 Tau	0.346	0.078	Maidanak
TYC 7845-1174-1	0.110	0.029	SMARTS	PreibZinn 9970	0.230	0.079	SMARTS
CHXR 40	0.100	0.030	SMARTS	TYC 8294-2230-1	0.230	0.079	SMARTS
PreibZinn 9913	0.100	0.030	SMARTS	L1551-51	0.258	0.079	Maidanak
PreibZinn 9945	0.100	0.030	SMARTS	V966 Cen	0.130	0.080	SMARTS
TYC 7783-1908-1	0.110	0.030	SMARTS	PreibZinn 9911	0.230	0.081	SMARTS
PreibZinn 9917	0.110	0.030	SMARTS	HD 105070	0.230	0.083	SMARTS

TABLE 11 (*Continued*)

Target	Peak to Peak	$\sigma_{st. dev.}$	Program	Target	Peak to Peak	$\sigma_{st. dev.}$	Program
TYC 8983-98-1	0.110	0.030	SMARTS	CHXR 29	0.260	0.083	SMARTS
PreibZinn 9958	0.090	0.031	SMARTS	TYC 7813-224-1	0.080	0.084	SMARTS
TYC 8295-1530-1	0.100	0.031	SMARTS	TYC 8982-3213-1	0.250	0.085	SMARTS
TYC 7822-158-1	0.110	0.031	SMARTS	IW Tau	0.238	0.086	Maidanak
TYC 7333-1260-1	0.110	0.031	SMARTS	V1056 Sco	0.230	0.087	SMARTS
V1009 Cen	0.090	0.032	SMARTS	TYC 9246-971-1	0.240	0.088	SMARTS
PreibZinn 9939	0.090	0.034	SMARTS	PreibZinn 9925	0.250	0.088	SMARTS
HD 140421	0.110	0.034	SMARTS	PreibZinn 9933	0.250	0.091	SMARTS
TYC 8263-2453-1	0.110	0.034	SMARTS	PreibZinn 9954	0.240	0.092	SMARTS
PreibZinn 9914	0.120	0.034	SMARTS	PreibZinn 9949	0.210	0.093	SMARTS
LkCa 19	0.163	0.034	Maidanak	TYC 8242-1324-1	0.320	0.094	SMARTS
TYC 8654-1115-1	0.120	0.035	SMARTS	PreibZinn 9980	0.260	0.097	SMARTS
TYC 8640-2515-1	0.130	0.035	SMARTS	PreibZinn 9942	0.290	0.097	SMARTS
PreibZinn 99-79	0.100	0.036	SMARTS	PreibZinn 9921	0.300	0.107	SMARTS
TYC 8683-242-1	0.110	0.036	SMARTS	HQ Tau	0.233	0.109	Maidanak
PreibZinn 9928	0.110	0.037	SMARTS	CI Tau	0.298	0.114	Maidanak
PreibZinn 9960	0.110	0.037	SMARTS	IP Tau	0.362	0.125	Maidanak
PreibZinn 9967	0.120	0.037	SMARTS	PreibZinn 9915	0.430	0.126	SMARTS
HII 1124	0.100	0.038	Maidanak	TYC 7817-622-1	0.380	0.127	SMARTS
PreibZinn 9927	0.140	0.038	SMARTS	BP Tau	0.457	0.129	Maidanak
PreibZinn 9962	0.140	0.038	SMARTS	UY Aur	0.350	0.130	Maidanak
RECX 6	0.150	0.038	SMARTS	SR 10	0.370	0.131	SMARTS
DN Tau	0.165	0.038	Maidanak	DoAr 21	0.310	0.134	SMARTS
PreibZinn 9936	0.110	0.039	SMARTS	DG Tau	0.606	0.138	Maidanak
CHXR 6	0.120	0.039	SMARTS	PreibZinn 9978	0.350	0.139	SMARTS
HD 120411	0.120	0.039	SMARTS	V836 Tau	0.417	0.142	Maidanak
RECX 10	0.120	0.039	SMARTS	HD 113466	0.390	0.149	SMARTS
TYC 8248-539-1	0.120	0.039	SMARTS	GK Tau	0.692	0.183	Maidanak
PreibZinn 9 22	0.110	0.040	SMARTS	PreibZinn 9973	0.550	0.188	SMARTS
TYC 8319-1687-1	0.120	0.040	SMARTS	DL Tau	0.723	0.212	Maidanak
PreibZinn 9971	0.140	0.040	SMARTS	DH Tau	0.537	0.214	Maidanak
HD 138995	0.150	0.040	SMARTS	GI Tau	0.597	0.216	Maidanak
L1551-55	0.126	0.041	Maidanak	TYC 8633-28-1	0.180	0.226	SMARTS
TYC 7833-2559-1	0.140	0.041	SMARTS	HD 108568	0.550	0.233	SMARTS
PreibZinn 9983	0.130	0.042	SMARTS	PreibZinn 9944	0.670	0.262	SMARTS
TWA 19	0.140	0.042	SMARTS	DR Tau	1.092	0.296	Maidanak
HD 117524	0.140	0.043	SMARTS	AA Tau	1.499	0.454	Maidanak
TYC 8644-802-1	0.140	0.043	SMARTS	TYC 8234-2856-1	0.170	0.495	SMARTS
CHXR 68A	0.150	0.043	SMARTS	TYC 8282-516-1	0.130	0.689	SMARTS
TYC 7851-1-1	0.120	0.044	SMARTS	RECX 2	2.150	0.808	SMARTS
TYC 8648-446-1	0.150	0.044	SMARTS	T Cha	2.430	0.850	SMARTS
PreibZinn 9950	0.120	0.045	SMARTS	HII 1136	1.841	1.127	Maidanak

servable most affecting the viability of the targets is photometric variability. To date, 22% of the stars (33% of those stars observed) in the target list have variability that contributes more than 3 μas of noise to the astrometric measurements. Table 3, which provides basic information on the entire *SIM*-YSO list, has been separated into “low variability,” “high variability,” and “not observed” sections, based on the degree of their variability and whether they have been observed to date. Each sublist is then ranked by the astrometric signal expected for a Jupiter-mass planet at a distance of 1 AU from the stars (listed in the column labeled “Signal”). To date, 67% of the sample has variability data, with the remainder expected to be completed within the next year or two.

To replace those stars that might be lost to photometric variability, we will examine the literature, looking for objects in other clusters and newly classified T Tauri stars. While many new young stars are being discovered in relatively nearby moving groups (e.g., Song et al. 2003), these typically have ages of 10–25 Myr. These stars can be observed inexpensively with *SIM*’s wide-angle mode and will probably not have problems of excessive variability. We will concentrate on finding bright enough replacement stars in the 1–5 Myr age range to avoid skewing our sample toward older stars.

7.1. Observing Scenarios and Reference Stars

While the nearer target stars ($d < 50$ pc) will have planetary astrometric signatures large enough to be detected by wide-angle observations, more distant or more massive stars will have astrometric signatures on the order of 6 μas, requiring

7

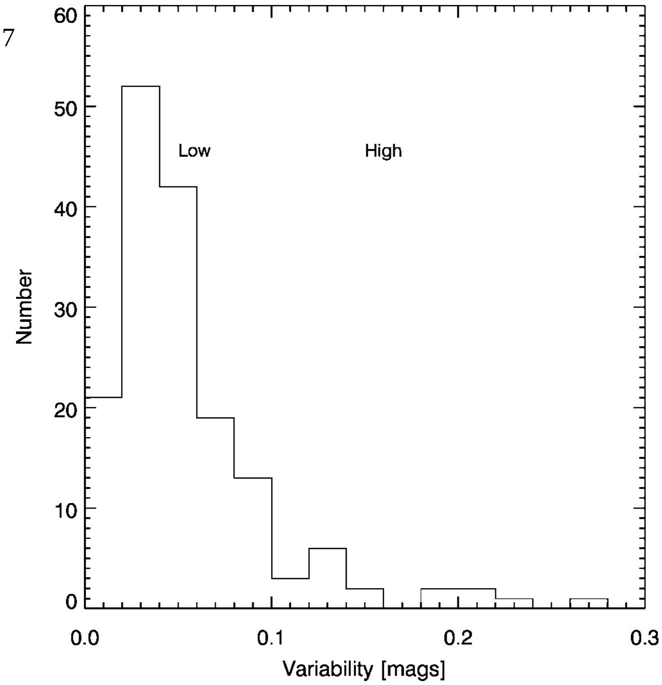

FIG. 9.—Histograms of the standard deviations of the flux variations observed in both the northern and southern photometry surveys. A deviation of >0.05 mag is considered too high for the *SIM*-YSO targets.

narrow-angle observations. Narrow-angle observations require that a set of at least three reference stars within the ~1.5° field of view be used for these observations. These reference stars must themselves be astrometrically stable to within <4 μas. The best reference stars are K giants at distances >500 pc. There is an additional precursor program currently making photometric observations of the pool of reference stars that are available for every *SIM*-YSO target (or clusters of targets). When choosing the reference stars, we used a combined 2MASS-Tycho 2 catalog to select K giants based on visible–near-IR colors and on reduced proper motions (RPMs). The following selection criteria were also used to make the initial lists of reference stars: (1) separation from target <1.25°, (2) $0.5 < (J - K_s) < 1.0$, (3) $1.0 < (B_{\rm Tycho} - V_{\rm Tycho}) < 1.5$, (4) $V_{\rm Tycho} < 10$, and (5) RPM $= K_s + 5 \log \mu < 1$. While some of the reference stars have published spectral types, many stars do not have any spectral type at all. We have begun a program of verification of the luminosity classes of the photometrically selected sample, using the SMARTS telescopes.

Observing the stars in narrow-angle mode requires roughly 5 times more integration time than doing so in wide-angle mode, primarily due to the necessity of observing three to five reference stars. Putting together the final program will require a balance between observing fainter, more distant, and young objects in narrow-angle mode versus the brighter, closer, and older stars in wide-angle mode.

8. CONCLUSIONS

We have presented the results for a number of precursor programs aimed at creating a robust list of young stars to be observed as part of a key project for the *SIM PlanetQuest* mission. This program will detect Jupiter-mass planets at distances of ~1–5 AU from the star, thereby probing planet formation at distances comparable to where radial velocity planets are found around mature main-sequence stars. The imaging surveys did not find any stars with bright nearby companions that could pose a problem for *SIM*, although we did find a potential M star companion 2.4″ away from GK Tau. The radial velocity surveys may have found one or two stars with close-in companions. In the near future, the RV surveys will be supplemented with high spectral resolution RV surveys in the near-infrared. These observations are not as affected by the photometric variability of the star and are expected to achieve rms accuracies down to 100 m^{-1}, thereby allowing for the detection of lower mass objects. One selection effect we will have to guard against is losing too many of the youngest stars due to large photometric variations. We will continue to supplement our target list with additional stars that meet our basic criteria, and also investigate ways to mitigate astrometric jitter using multiwavelength data from *SIM* itself.

We acknowledge many useful and formative discussions with other members of the *SIM*-YSO Science Team, including A. Boden, L. Hartmann, J. Lunine, J. Stauffer, and T. Velusamy. L. P. and M. H. thank our colleagues C. Johns-Krull, P. Hartigan, and D. Jaffe for their collaboration on the McDonald Observatory project. Based on observations obtained at the Hale Telescope, Palomar Observatory, as part of a continuing collaboration between the California Institute of Technology, the NASA Jet Propulsion Laboratory, and Cornell University. The research described in this publication was carried out at the Jet Propulsion Laboratory, California Institute of Technology, under a contract with the National Aeronautics and Space Administration. This publication makes use of data products from the Two Micron All Sky Survey, which is a joint project of the University of Massachusetts and the Infrared Processing and Analysis Center, California Institute of Technology, funded by the National Aeronautics and Space Administration and the National Science Foundation.

REFERENCES

Akeson, R. L., et al. 2005, ApJ, 635, 1173
Baraffe, I., Chabrier, G., Allard, F., & Hauschildt, P. H. 1998, A&A, 337, 403
Baraffe, I., Chabrier, G., Barman, T. S., Allard, F., & Hauschildt, P. H. 2003, A&A, 402, 701

Beichman, C. A. 2001, in ASP Conf. Ser. 244, Young Stars Near Earth: Progress and Prospects, ed. R. Jayawardhana & T. Greene (San Francisco: ASP), 376
Boss, A. P. 2001, ApJ, 563, 367
Bouvier, J., Rigaut, F., & Nadeau, D. 1997, A&A, 323, 139
Bouvier, J., Covino, E., Kovo, O., Martin, E. L., Matthews, J. M., Terranegra, L., & Beck, S. C. 1995, A&A, 299, 89
Bouvier, J., & Bertout, C. 1989, A&A, 211, 99
Brandner, W., et al. 2000, AJ, 120, 950
Burrows, A., et al. 1997, ApJ, 491, 856
Butler, R. P., et al. 2006, ApJ, 646, 505
Catanzarite, J., Shao, M., Tanner, A., Unwin, S., & Yu, J. 2006, PASP, 118, 1322
Chauvin, G., et al. 2005, A&A, 438, L29
Chauvin, G., Lagrange, A.-M., Dumas, C., Zuckerman, B., Mouillet, D., Song, I., Beuzit, J.-L., & Lowrance, P. 2004, A&A, 425, L29
Colavita, M., et al. 2003, ApJ, 592, L83
Cutri, R. M., et al. 2003, The IRSA 2MASS All-Sky Point Source Catalog (NASA/IPAC Infrared Science Archive; Washington: NASA), http://irsa.ipac.caltech.edu/applications/Gator
D'Antona, F., & Mazzitelli, I. 1994, ApJS, 90, 467
Eiroa, C., et al. 2002, A&A, 384, 1038
Frink, S., Röser, S., Neuhäuser, R., & Sterzik, M. F. 1997, A&A, 325, 613
Ghez, A. M., Neugebauer, G., & Matthews, K. 1993, AJ, 106, 2005
Grankin, K. N., Melnikov, S. Y., Bouvier, J., Herbst, W., & Shevchenko, V. S. 2007, A&A, 461, 183
Hayward, T. L., Brandl, B., Pirger, B., Blacken, C., Gull, G. E., Schoenwald, J., & Houck, J. R. 2001, PASP, 113, 105
Herbst, W., Herbst, D. K., Grossman, E. J., & Weinstein, D. 1994, AJ, 108, 1906
Huerta, M., Prato, L., Hartigan, P., Johns-Krull, C. M., & Jaffe, D. 2005, BAAS, 37, 1267
Kenyon, S. J., Dobrzycka, D., & Hartmann, L. 1994, AJ, 108, 1872
Konopacky, Q. M., Ghez, A. M., Rice, E. L., & Duchene, G. 2007, ApJ, 663, 394
Krist, J. E., Stapelfeldt, K. R., Ménard, F., Padgett, D. L., & Burrows, C. J. 2000, ApJ, 538, 793
Ida, S., & Lin, D. N. C. 2004, ApJ, 616, 567
Law, N. M., Hodgkin, S. T., & Mackay, C. D. 2006, MNRAS, 368, 1917
Lin, D. 2001, in ASP Conf. Ser. 245, Astrophysical Ages and Times Scales, ed. T. von Hippel, C. Simpson, & N. Manset (San Francisco: ASP), 90
Lowrance, P. J., et al. 2005, AJ, 130, 1845
Marcy, G. W., & Butler, R. P. 2000, PASP, 112, 137
Mathieu, R. D., Stassun, K., Basri, G., Jensen, E. L. N., Johns-Krull, C. M., Valenti, J. A., & Hartmann, L. W. 1997, AJ, 113, 1841
Mekkaden, M. V. 1998, A&A, 340, 135
Metchev, S. 2006, Ph.D. Thesis, Caltech
Metchev, S. A., & Hillenbrand, L. A. 2004, ApJ, 617, 1330
Neuhäuser, R., Guenther, E. W., Wuchterl, G., Mugrauer, M., Bedalov, A., & Hauschildt, P. H. 2005, A&A, 435, L13
Pan, S., Shao, M., & Kulkarni, S. 2004, Nature, 427, 326
Preibisch, T., & Zinnecker, H. 1999, AJ, 117, 2381
Pollack, J. B., Hubickyj, O., Bodenheimer, P., Lissauer, J. J., Podolak, M., & Greenzweig, Y. 1996, Icarus, 124, 62
Schuessler, M., Caligari, P., Ferriz-Mas, A., Solanki, S. K., & Stix, M. 1996, A&A, 314, 503
Song, I., Zuckerman, B., & Bessell, M. S. 2003, ApJ, 599, 342
Sozzetti, A., Casertano, S., Brown, R. A., & Lattanzi, M. G. 2003, PASP, 115, 1072
Stauffer, J. R., Schild, R., Barrado y Navascues, D., Backman, D. E., Angelova, A. M., Kirkpatrick, J. D., Hambly, N., & Vanzi, L. 1998, ApJ, 504, 805
Steffen, A. T., et al. 2001, AJ, 122, 997
Strassmeier, K. G., & Rice, J. B. 1998, A&A, 339, 497
Unwin, S. C. 2005, in ASP Conf. Ser. 338, Astrometry in the Age of the Next Generation of Large Telescopes, ed. P. K. Seidelmann & A. K. B. Monet (San Francisco: ASP), 37
White, R. J., & Ghez, A. M. 2001, ApJ, 556, 265
Wuchterl, G., & Tscharnuter, W. M. 2003, A&A, 398, 1081